Modified two-photon absorption and dispersion of ultrafast third-order polarization beats via twin noisy driving fields

Yanpeng Zhang,[1,2,*] Chenli Gan,[1] and Min Xiao[1,†]
[1]*Department of Physics, University of Arkansas, Fayetteville, Arkansas 72701, USA*
[2]*Department of Electronic Science and Technology, Xi'an Jiaotong University, Xi'an 710049, China*
(Received 7 January 2006; published 1 May 2006)

We investigate the color-locked twin-noisy-field correlation effects in third-order nonlinear absorption and dispersion of ultrafast polarization beats. We demonstrate a phase-sensitive method for studying the two-photon nondegenerate four-wave mixing (NDFWM) due to atomic coherence in a multilevel system. The reference signal is another one-photon degenerate four-wave-mixing signal, which propagates along the same optical path as the NDFWM signal. This method is used for studying the phase dispersion of the third-order susceptibility and for the optical heterodyne detection of the NDFWM signal. The third-order nonlinear response can be controlled and modified through the color-locked correlation of twin noisy fields.

DOI: 10.1103/PhysRevA.73.053801 PACS number(s): 42.65.Sf, 42.65.Re, 32.80.Qk

I. INTRODUCTION

Recently, studies of nonlinear optical effects in multilevel atomic systems have received renewed interest due to the greatly enhanced nonlinearity and, at the same time, reduced linear absorption caused by light-induced atomic coherence among the energy levels [1–3]. By carefully choosing the atomic level configurations and laser fields, the efficiencies of wave mixing can be greatly increased at optimal atomic coherence conditions. Through directly measuring the nonlinear optical coefficients in multilevel atomic systems [4], one can see that the nonlinearity depends sensitively on various experimental parameters. Large enhancement of the nonlinear index in four-level atomic systems was also demonstrated [5]. In order to optimize certain nonlinear optical processes, it is beneficial to have exact knowledge of the nonlinear coefficients and their dependences on various experimental parameters. However, due to residual linear absorption and dispersion of the probe and signal beams, it is usually difficult to measure the nonlinear coefficients, especially both the real and imaginary parts under the same conditions. One of the early experiments to measure the Kerr nonlinear coefficient in a three-level atomic system used an optical cavity to eliminate the linear contributions [4], which directly gives the nonlinear refractive index n_2.

In this paper we present a type of phase-sensitive detection for the third-order complex susceptibility in a multilevel gas medium. We study two-photon nondegenerate four-wave mixing (NDFWM) in attosecond polarization beats induced by the third-order susceptibility. One can adjust the relative phase between the local oscillator field of one-photon degenerate four-wave mixing (DFWM) and the two-photon NDFWM signal by changing the relative time delay (τ) between two pump beams of DFWM and NDFWM through a Michelson interferometer. As the τ-dependent phase difference approaches $2n\pi$ or $(2n+1/2)\pi$, the attosecond polarization beat signal evolves into the nonlinear dispersion or absorption of two-photon NDFWM separately. Here the reference beam is another one-photon DFWM signal, which is introduced by adding an additional frequency component to the pump beams of the NDFWM scheme. The NDFWM signal beam and the DFWM reference beam then interfere directly at the detector. Our method is based on attosecond polarization interference between two FWM processes in a purely homogeneously broadened [6,7] or Doppler-broadened three-level ladder-type system [8–10].

This method is a good way to measure the third-order susceptibility directly. Alternative methods (in the purely homogeneously broadened and the extremely Doppler-broadened media, respectively) are used to study the nonlinear responses of the three-level ladder-type system. We proceed in the standard manner by calculating the expression for the density-matrix element (third-order response functions $\rho_{10}^{(3)}$), finding the complex susceptibility, and finally breaking it down into real and imaginary parts to obtain the desired results. The modified third-order absorption and dispersion can be controlled coherently by noisy-light color-locking bandwidth, frequency detuning, and time delay. Another advantage of our system is the use of a two-photon Doppler-free counterpropagation configuration [9,10] that allows us to observe these interesting effects in a long atomic vapor cell.

II. LIOUVILLE PATHWAYS

Nonlinear optical properties of an atomic medium can be controlled and modified through the color-locked correlation of twin noisy driving fields. A simply physical explanation of this process in a three-level ladder-type atomic system can be given in the bare-state picture. The polarization interference of two excitation paths $|0\rangle \rightarrow |1\rangle \rightarrow |0\rangle \rightarrow |1\rangle$ (one-photon DFWM) and $|0\rangle \rightarrow |1\rangle \rightarrow |2\rangle \rightarrow |1\rangle$ (two-photon NDFWM) leads to a third-order attosecond polarization beat (ASPB) phenomenon [7,8,10]. This polarization beat is based on the interference at the detector between FWM signals which originate from macroscopic polarizations excited simulta-

*Email address: ypzhang@mail.xjtu.edu.cn
†Email address: mxiao@uark.edu

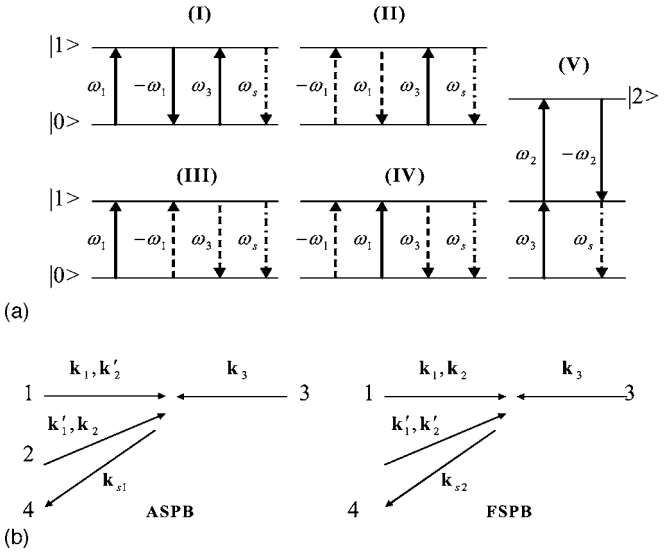

FIG. 1. (a) The ladder diagrams of two-state one-photon DFWM and three-state two-photon NDFWM for perturbation chains I–V in Liouville space. The solid, dashed, and dash-dotted vertical lines correspond to ket and bra interactions, and the FWM signal, respectively, and time evolves from left to right. (b) Phase-conjugation geometries of ASPB and FSPB.

neously in the homogeneously [6,7] or inhomogeneously [8–10] broadened sample. It critically requires that all the third-order polarizations have the same frequency.

The three-level ladder-type ASPB comes from the sum-frequency polarization interference between one-photon and two-photon optical processes on the attosecond time scale, while the femtosecond polarization beat (FSPB) corresponds to the difference-frequency polarization interference on the femtosecond time scale [9]. A Doppler-broadened three-level ladder-type atomic system [Fig. 1(a)] consists of a ground state $|0\rangle$, an intermediate state $|1\rangle$, and an excited state $|2\rangle$. States between $|0\rangle$ and $|1\rangle$ and between $|1\rangle$ and $|2\rangle$ are coupled by a dipole transition with resonant frequencies Ω_1 and Ω_2, respectively, while states between $|0\rangle$ and $|2\rangle$ are dipole forbidden. We consider a two-color time-delay FWM in which beams 1 and 2 consist of two frequency components ω_1 and ω_2, while beam 3 has frequency ω_3 [Fig. 1(b)]. We further assume that $\omega_1 \approx \Omega_1$ ($\omega_3 \approx \Omega_1$) and $\omega_2 \approx \Omega_2$; therefore ω_1 (ω_3) and ω_2 will drive the transitions from $|0\rangle$ to $|1\rangle$ and from $|1\rangle$ to $|2\rangle$, respectively. There are two distinct processes involved in this two-color ASPB. First, the ω_1 frequency components of the twin composite beams 1 and 2 induce population grating of states $|0\rangle$ and $|1\rangle$, which is probed by frequency ω_3 of beam 3. This is a one-photon resonant DFWM (one typical pathway $|0\rangle \overset{\omega_1}{\rightarrow} |1\rangle \overset{-\omega_1}{\rightarrow} |0\rangle \overset{\omega_3}{\rightarrow} |1\rangle$) and the signal (beam 4) has frequency ω_3. More specifically, the typical one-photon DFWM process indicates that one pump photon ω_1 is absorbed and one pump photon ω_1 is emitted first [both the ket and bra of the density operator would be promoted to $|0\rangle$ (or $|1\rangle$) to create a population of a ground state (or an intermediate state)], one probe photon ω_3 is then absorbed, and one phase-matching coherent photon ω_3 is finally emitted along beam 4 [Fig. 1(b)]. Second, beam 3 and the ω_2 frequency component of beam 1 induce a two-photon coherence between levels $|0\rangle$ and $|2\rangle$ (only the ket is being promoted to create a coherence rather than a population), which is then probed by the ω_2 frequency component of the beam 2. This is a two-photon NDFWM ($|0\rangle \overset{\omega_3}{\rightarrow} |1\rangle \overset{\omega_2}{\rightarrow} |2\rangle \overset{-\omega_2}{\rightarrow} |1\rangle$) with a resonant intermediate state and the frequency of the signal equals ω_3 again. The two-photon NDFWM process indicates that the ket is promoted to the excited state $|2\rangle$ by two field actions, one probe photon ω_2 is emitted, and then one phase-matching coherent photon ω_3 is finally emitted along the beam 4 direction [Fig. 1(b)]. Thus, the first two field actions would imply that both the ket and bra would be promoted to $|0\rangle$ (or $|1\rangle$) to create a population of a ground state (or an intermediate state) in chains I–IV; only the ket is being promoted to create a coherence (between a ground state and an excited state) rather than a population in chain V.

The twin composite stochastic fields of beam 1 (E_{p1}) and beam 2 (E_{p2}) can be written as

$$E_{p1} = E_1 + E_2' = \varepsilon_1 u_1(t)\exp[i(\mathbf{k}_1 \cdot \mathbf{r} - \omega_1 t)] + \varepsilon_2' u_2(t-\tau)\exp[i(\mathbf{k}_2' \cdot \mathbf{r} - \omega_2 t + \omega_2 \tau)], \quad (1)$$

$$E_{p2} = E_1' + E_2 = \varepsilon_1' u_1(t-\tau)\exp[i(\mathbf{k}_1' \cdot \mathbf{r} - \omega_1 t + \omega_1 \tau)] + \varepsilon_2 u_2(t)\exp[i(\mathbf{k}_2 \cdot \mathbf{r} - \omega_2 t)]. \quad (2)$$

Here, ε_i, and $\mathbf{k}_i$ (ε_i' and $\mathbf{k}_i'$) are the constant field amplitude and the wave vector of the ω_i component in beam 1 (beam 2), respectively. $u_i(t)$ is a dimensionless statistical factor that contains phase and amplitude fluctuations. It is taken to be a complex ergodic stochastic function of t, which obeys complex circular Gaussian statistics in a chaotic field. τ is the relative time delay between the prompt (unprimed) and delayed (primed) fields. To accomplish this arrangement the frequency components of the ω_1 and ω_2 lights are split and then recombined to provide two double-frequency pulses in such a way that the ω_1 component is delayed by τ in beam 2 and the ω_2 component delayed by the same amount in beam 1 [Fig. 1(b)]. The time delay τ is introduced in both beams, which is quite different from the FSPB scheme studied earlier [9]. On the other hand, beam 3 is assumed to be a quasi-monochromatic light [$u_3(t) \approx 1$], the complex electric field of beam 3 can be written as $E_3 = A_3(\mathbf{r},t)\exp(-i\omega_3 t) = \varepsilon_3 u_3(t)\exp[i(\mathbf{k}_3 \cdot \mathbf{r} - \omega_3 t)]$. Here, ω_3, ε_3, and $\mathbf{k}_3$ are the frequency, the field amplitude, and the wave vector, respectively.

In the bare-state picture, the atomic polarization and population equations of motion (atomic response) are considered up to different orders of Liouville pathways. To proceed further, and to simplify the mathematics, we will neglect the ground-state depletion ($\rho_{00}^{(0)} \approx 1$) and not consider the propagation characteristics of the pulsed pump, probe, and FWM fields. Also, we only retain the resonant dipole interaction terms in the derivation of the complex susceptibility, known as the rotating-wave approximation (RWA). Because of the selectivity imposed by the RWA, each pulse interaction contributes in a unique way to the phase-matching direction of

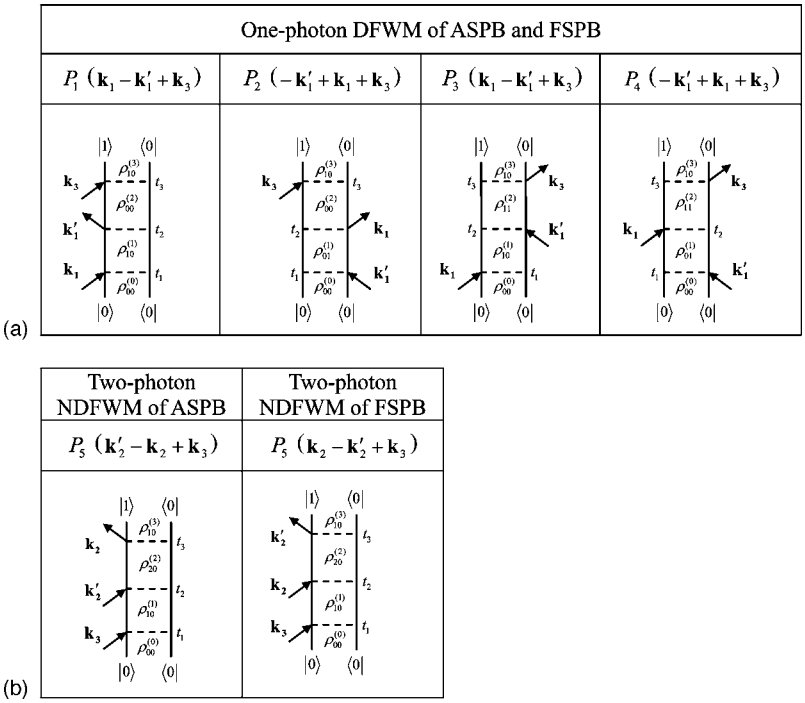

FIG. 2. Pulse sequence control of third-order response functions representing the Liouville pathways for P_1, P_2, P_3 P_4, and P_5, respectively. (a) One-photon DFWM of ASPB and FSPB; (b) two-photon NDFWM of ASPB and FSPB. The left and right vertical lines represent the ket and bra, respectively; the applied electric fields are indicated with arrows oriented toward the left if propagating with a negative wave vector and vice versa for a positive wave vector. Time evolves from the bottom to the top of the diagram.

the nonlinear signal. We shall employ perturbation theory to calculate the density-matrix elements by the following perturbation chains (Fig. 2) [10]:

$$\text{(I)}\quad \rho_{00}^{(0)} \xrightarrow{E_1} \rho_{10}^{(1)} \xrightarrow{(E_1')^*} \rho_{00}^{(2)} \xrightarrow{E_3} \rho_{10}^{(3)},$$

$$\text{(II)}\quad \rho_{00}^{(0)} \xrightarrow{(E_1')^*} (\rho_{10}^{(1)})^* \xrightarrow{E_1} \rho_{00}^{(2)} \xrightarrow{E_3} \rho_{10}^{(3)},$$

$$\text{(III)}\quad \rho_{00}^{(0)} \xrightarrow{E_1} \rho_{10}^{(1)} \xrightarrow{(E_1')^*} \rho_{11}^{(2)} \xrightarrow{E_3} \rho_{10}^{(3)},$$

$$\text{(IV)}\quad \rho_{00}^{(0)} \xrightarrow{(E_1')^*} (\rho_{10}^{(1)})^* \xrightarrow{E_1} \rho_{11}^{(2)} \xrightarrow{E_3} \rho_{10}^{(3)},$$

$$\text{(V)}\quad \rho_{00}^{(0)} \xrightarrow{E_3} \rho_{10}^{(1)} \xrightarrow{E_2'} \rho_{20}^{(2)} \xrightarrow{(E_2)^*} \rho_{10}^{(3)}.$$

Chains I–IV correspond to the one-photon DFWM processes, while chain V corresponds to the two-photon NDFWM process. They have phase-matching conditions $\mathbf{k}_{s1}=\mathbf{k}_1-\mathbf{k}_1'+\mathbf{k}_3$ and $\mathbf{k}_{s2}=\mathbf{k}_2'-\mathbf{k}_2+\mathbf{k}_3$, respectively. Since the DFWM and NDFWM signals propagate along slightly different directions, the interference between them leads to the spatial oscillation [6–10]. Physically, DFWM is one sum of two grating diffraction contributions [a small-angle static grating induced by ω_1 and $-\omega_1$ and a large-angle static grating induced by ω_3 ($\approx\omega_1$) and $-\omega_1$], while NDFWM comes from the other sum of the two grating diffraction contributions (a small-angle static grating induced by ω_2 and $-\omega_2$ and a large-angle moving grating induced by ω_3 and $-\omega_2$).

The third-order response functions ($\rho_{10}^{(3)}$) of the perturbation chains I–V (relevant to the three-pulse FWM) are given using double-sided Feynman diagrams (DSFDs) in Fig. 2 [7,10]. The time evolutions of the density-matrix elements of the optically driven atoms or molecules can be represented schematically by either the Liouville space coupling representation (chains I–V), the DSFDs (Fig. 2), or the ladder diagrams [Fig. 1(a)]. Each diagram represents a distinct Liouville space pathway. We show the diagrammatic representations corresponding to the lowest three orders of the resonant dipole interactions applied to a system with two or three electronic states. In the Liouville space coupling representation (chains I–V) the state of the system is designated by a position in Liouville space, with indices corresponding to the ket-bra "axis." Up and down transitions on the ket are excited by positive- and negative-frequency fields, whereas negative- and positive-frequency fields induce up and down transitions on the bra. The DSFDs shown in Fig. 2 can be described as follows. The vertical left and right lines of the diagram represent the time evolution (bottom to top) of the ket and bra, respectively; the applied electric fields are indicated with arrows oriented toward the left if propagating with a negative wave vector and toward the right for a positive wave vector. Each interaction with the electric field produces a transition between the two electronic states of either the bra or the ket. The ladder diagrams are shown in Fig. 1(a). In this representation, the solid and dashed lines correspond to ket and bra interactions, respectively, and its time evolves from left to right. The ability to track the evolution of the bra and ket simultaneously makes the density-matrix representation a most appropriate tool for the description of many dynamical phenomena in nonlinear optical processes.

Generally, there are 48 terms in the third-order density operators for a given FWM process. In time evolution of the density-matrix element $\rho_{ab}^{(j)}$, each specified field action transforms either the "ket" or the "bra" side of the density-matrix element. Thus, for any specified jth-order generator, there can be 2^j detailed paths of evolution. In addition, evolution for each of the $j!$ generators corresponding to all possible

field orderings must be considered. One then has total $2^j j!$ paths of evolution. Thus, at third order, where beams 1, 2, and 3 are distinct, there are $2^j j! = 48$ $(j=3)$ different Liouville pathways at the polarization level. Often the experimental constraints reduce the number of diagrams to a significantly smaller subset which dominate the behavior of the signal. Under the RWA, phase-matching and frequency selections of the FWM signals along $\mathbf{k}_s$ greatly restrict the number of third-order perturbative pathways (Fig. 2). Moreover, polarization beat is based on the interference at the detector between multi-FWM signals, which originate from the macroscopic polarizations excited simultaneously in the sample. It requires that all the polarizations have the same frequency. Now, we consider the other possible density-operator pathways:

$$\text{(VI)} \quad \rho_{00}^{(0)} \xrightarrow{E_3} \rho_{10}^{(1)} \xrightarrow{(E_1')^*} \rho_{00}^{(2)} \xrightarrow{E_1} \rho_{10}^{(3)},$$

$$\text{(VII)} \quad \rho_{00}^{(0)} \xrightarrow{(E_1')^*} (\rho_{10}^{(1)})^* \xrightarrow{E_3} \rho_{00}^{(2)} \xrightarrow{E_1} \rho_{10}^{(3)},$$

$$\text{(VIII)} \quad \rho_{00}^{(0)} \xrightarrow{E_3} \rho_{10}^{(1)} \xrightarrow{(E_1')^*} \rho_{11}^{(2)} \xrightarrow{E_1} \rho_{10}^{(3)},$$

$$\text{(IX)} \quad \rho_{00}^{(0)} \xrightarrow{(E_1')^*} (\rho_{10}^{(1)})^* \xrightarrow{E_3} \rho_{11}^{(2)} \xrightarrow{E_1} \rho_{10}^{(3)},$$

$$\text{(X)} \quad \rho_{00}^{(0)} \xrightarrow{E_1} \rho_{10}^{(1)} \xrightarrow{E_2'} \rho_{20}^{(2)} \xrightarrow{(E_2)^*} \rho_{10}^{(3)},$$

$$\text{(XI)} \quad \rho_{00}^{(0)} \xrightarrow{E_1'} \rho_{10}^{(1)} \xrightarrow{E_2'} \rho_{20}^{(2)} \xrightarrow{(E_2)^*} \rho_{10}^{(3)}.$$

where the population grating (a large-angle static grating) induced by beam 3 and the ω_1 frequency component of beam 2 is responsible for the generation of the FWM signal. These large-angle static gratings have much smaller fringe spacings, which equal approximately one-half of the wavelengths of the incident lights $\{\lambda_i/[2\sin(\theta/2)] \xrightarrow{\theta\approx 180^\circ} \lambda_i/2\}$. For a Doppler-broadened system, the gratings will be washed out by the atomic motion. In addition, the wave vectors $\mathbf{k}_2'-\mathbf{k}_2+\mathbf{k}_1$ and $\mathbf{k}_2'-\mathbf{k}_2+\mathbf{k}_1'$ of the density-operator pathways X and XI propagate along dramatically different directions compared with $\mathbf{k}_{s1}=\mathbf{k}_1-\mathbf{k}_1'+\mathbf{k}_3$ and $\mathbf{k}_{s2}=\mathbf{k}_2'-\mathbf{k}_2+\mathbf{k}_3$. Therefore, it is appropriate to neglect the FWM signals from these density-operator pathways. The more strict requirements on phase matching also make these processes (VI–XI) unimportant.

III. COLOR-LOCKING STOCHASTIC CORRELATION

Lasers are inherently noisy devices, in which both the phase and amplitude of the field can fluctuate. A noisy laser beam can be used to probe atomic and molecular dynamics, and it offers a unique alternative to the more conventional frequency-domain cw spectroscopies and ultrashort-pulse time-domain spectroscopies [11]. Typical Markovian noisy fields include chaotic fields, phase-diffusion fields, and Gaussian-amplitude fields [7,10]. The color-locking noisy-light technique is an intermediate way between cw and short-pulse methods. The color-locking technique results in complete cancellation of the spectrally broad noise carried by the noisy light beams [11]. The fundamental difference is that the transform-limited femtosecond laser pulse is phase coherent (phase locked) while noisy light is phase random and nontransform limited. For the "biatomic" model [11] of the macroscopic system where phase matching takes place, the FWM signal must be drawn from the third-order polarization $P^{(3)}$ (having time variable t) developed on one "atom" multiplied by $(P^{(3)})^*$ (having time variable s) that is developed on another "atom" which must be located elsewhere in space (with summation over all such pairs). The third-order response functions $(P^{(3)})$ relevant to three-pulse FWM are given using double-sided Feynman diagrams as shown in Fig. 2. The homodyne-detected ASPB signal is proportional to the average of the absolute square of $P^{(3)}$ over the random variable of the stochastic process $\langle|P^{(3)}|^2\rangle$ (having both t and s time variables), which involves fourth- or sixth-order coherence functions of $u_i(t)$ in phase-conjugation geometry. Unlike the second-order coherence function in field-level averaging, the expansions of fourth- and sixth-order coherence functions in intensity-level averaging strongly depend on three different Markovian noisy fields [7,10].

The characteristics of the ASPB interferogram are a result of two main components: the material response and the light response along with the interplay between the two responses. In general, ASPB (at the intensity level) can be viewed as the sum of five contributions: (i) the resonant-resonant, nonresonant-nonresonant, or resonant-nonresonant types of τ-independent autocorrelation terms, (ii) the purely resonant τ-dependent autocorrelation terms, (iii) the purely nonresonant τ-dependent autocorrelation terms, (iv) the resonant-nonresonant τ-dependent autocorrelation terms, and (v) the resonant-resonant, nonresonant-nonresonant, or resonant-nonresonant types of τ-dependent cross-correlation terms. When the ASPB signal is dominated by the case that the $u_1(t)$ and $u_2(t)$ (field 3 is quasimonochromatic) field actions on single atom are correlated, and the cross-atom-correlated actions are not important (which is usually true for atomic vapor systems), the ASPB signal intensity can be approximated by the absolute square of the nontrivial stochastic average of the polarization $|\langle P^{(3)}\rangle|^2$ (averaging at the field level), which only involves second-order coherence functions of $u_i(t)$. This works because for this particular spectroscopic technique the τ-dependent terms have only intra-atomic correlations and no interatomic correlations in the τ-dependent terms. In dealing with a gas-phase atomic medium, we made an approximation by averaging at the field level, which only needs second-order correlation functions for the noise fields. The time-space second-order coherence function of a noisy field is $\langle u_i(t_1)u_i^*(t_2)\rangle = \exp(-\alpha_i|t_1-t_2|)$ for a Lorentzian line shape and $\langle u_i(t_1)u_i^*(t_2)\rangle = \exp\{-[\alpha_i(t_1-t_2)/2\sqrt{\ln 2}]^2\}$ for a Gaussian line shape. Here, $\alpha_i=\frac{1}{2}\delta\omega_i$ (with $\delta\omega_i$ being the linewidth of the ω_i frequency component) is the autocorrelation decay of the noisy field. On the other hand, noisy light is color locked, because each color is

coherent only with itself (it is uncorrelated with any other color). Color locking is a consequence of the Wiener-Khintchine theorem, which is expressed mathematically (most conveniently) by examining a second-order coherence function in the frequency domain, i.e., $\langle \tilde{u}_i(\omega_j)\tilde{u}_i^*(\omega_k)\rangle = \delta(\omega_j - \omega_k)J_i(\omega_j)$, where $\tilde{u}_i$ is the Fourier transform of the broadband light field envelope and J_i is the spectral density of the stochastic function u_i [11]. The form of the second-order coherence function, which is determined by the laser line shape, is a general feature of three different Markovian stochastic models: a chaotic field, phase-diffusion field, and Gaussian-amplitude field [7,10]. In the cw limit $[u_i(t) \approx 1]$, the ASPB signal can then be written as $I \propto |P^{(3)}|^2 = |\langle P^{(3)}\rangle|^2 = \langle |P^{(3)}|^2\rangle$.

The nonlinear polarization P_n responsible for the phase-conjugate FWM signal is given by stochastic averaging over the velocity distribution function $W(\mathbf{v})$. Thus $P_n = N\mu_1 \int_{-\infty}^{+\infty} d\mathbf{v}\, w(\mathbf{v})\langle \rho_{10}^{(3)}(\mathbf{v})\rangle$. Here $\mathbf{v}$ is the atomic velocity and N is the atomic density. For a Doppler-broadened atomic system, we have $w(\mathbf{v}) = \exp[-(\mathbf{v}/u)^2]/\sqrt{\pi}u$. Here, $u = \sqrt{2k_BT/m}$ with m being the mass of an atom, k_B the Boltzmann constant, and T the absolute temperature. The polarizations of DFWM ($P_A = P_1 + P_2 + P_3 + P_4$) and NDFWM ($P_B = P_5$) are given in the bare-state basis. P_1, P_2, P_3, P_4, and P_5 correspond to third-order polarizations of the perturbation chains I, II, III, IV, and V, respectively. The formulas below indicate how the initial density-matrix elements are transformed into higher-order elements through interactions with the electric fields:

$$P_1 = S_1(\mathbf{r})\exp[-i(\omega_3 t + \omega_1 \tau)] \int w(\mathbf{v})\exp[-i\theta_I(\mathbf{v})]H_1(t_1) \times H_2(t_2)H_3(t_3)\langle u_1(t - t_1 - t_2 - t_3)u_1^*(t - t_2 - t_3 - \tau)\rangle d\Sigma, \tag{3}$$

$$P_2 = S_1(\mathbf{r})\exp[-i(\omega_3 t + \omega_1 \tau)] \int w(\mathbf{v})\exp[-i\theta_{II}(\mathbf{v})]H_1^*(t_1) \times H_2(t_2)H_3(t_3)\langle u_1(t - t_2 - t_3)u_1^*(t - t_1 - t_2 - t_3 - \tau)\rangle d\Sigma, \tag{4}$$

$$P_3 = S_1(\mathbf{r})\exp[-i(\omega_3 t + \omega_1 \tau)] \int w(\mathbf{v})\exp[-i\theta_I(\mathbf{v})]H_1(t_1) \times H_4(t_2H_3(t_3)\ \langle u_1(t - t_1 - t_2 - t_3)u_1^*(t - t_2 - t_3 - \tau)\rangle d\Sigma, \tag{5}$$

$$P_4 = S_1(\mathbf{r})\exp[-i(\omega_3 t + \omega_1 \tau)] \int w(\mathbf{v})\exp[-i\theta_{II}(\mathbf{v})]H_1^*(t_1) \times H_4(t_2)H_3(t_3)\langle u_1(t - t_2 - t_3)u_1^*(t - t_1 - t_2 - t_3 - \tau)\rangle d\Sigma, \tag{6}$$

$$P_5 = S_2(\mathbf{r})\exp[-i(\omega_3 t - \omega_2 \tau)] \int w(\mathbf{v})\exp[-i\theta_{III}(\mathbf{v})]H_3(t_1) \times H_5(t_2)H_3(t_3)\langle u_2(t - t_2 - t_3 - \tau)u_2^*(t - t_3)\rangle d\Sigma. \tag{7}$$

here

$$S_1(\mathbf{r}) = -i\hbar N\left(\frac{\mu_1}{\hbar}\right)^4 \varepsilon_1(\varepsilon_1')^*\varepsilon_3 \exp[i(\mathbf{k}_1 - \mathbf{k}_1' + \mathbf{k}_3)\cdot\mathbf{r}],$$

$$S_2(\mathbf{r}) = -i\hbar N\left(\frac{\mu_1}{\hbar}\right)^2\left(\frac{\mu_2}{\hbar}\right)^2 \varepsilon_2'(\varepsilon_2)^*\varepsilon_3 \exp[i(\mathbf{k}_2' - \mathbf{k}_2 + \mathbf{k}_3)\cdot\mathbf{r}],$$

$$\theta_I(\mathbf{v}) = \mathbf{v}\cdot[\mathbf{k}_1(t_1 + t_2 + t_3) - \mathbf{k}_1'(t_2 + t_3) + \mathbf{k}_3 t_3],$$

$$\theta_{II}(\mathbf{v}) = \mathbf{v}\cdot[-\mathbf{k}_1'(t_1 + t_2 + t_3) + \mathbf{k}_1(t_2 + t_3) + \mathbf{k}_3 t_3],$$

$$\theta_{III}(\mathbf{v}) = \mathbf{v}\cdot[\mathbf{k}_3(t_1 + t_2 + t_3) + \mathbf{k}_2'(t_2 + t_3) - \mathbf{k}_2 t_3],$$

$$H_1(t) = \exp[-(\Gamma_{10} + i\Delta_1)t], \quad H_2(t) = \exp(-\Gamma_0 t),$$

$$H_3(t) = \exp[-(\Gamma_{10} + i\Delta_3)t], \quad H_4(t) = \exp(-\Gamma_1 t),$$

$$H_5(t) = \exp[-(\Gamma_{20} + i\Delta_2 + i\Delta_3)t];$$

μ_1 (μ_2) is the dipole-moment matrix element between $|0\rangle$ and $|1\rangle$ ($|1\rangle$ and $|2\rangle$); Γ_0 (Γ_1) is the population relaxation rate of state $|0\rangle$ ($|1\rangle$). By considering contributions of nonradiative processes in such a gas-phase medium, we assume Γ_0 to be small, but nonzero. Γ_{10} (Γ_{20}) is the transverse relaxation rate of the transition from $|0\rangle$ to $|1\rangle$ ($|0\rangle$ to $|2\rangle$), which contains material dephasing dynamics; $\Delta_1 = \Omega_1 - \omega_1$, $\Delta_2 = \Omega_2 - \omega_2$, $\Delta_3 = \Omega_1 - \omega_3$; $\int d\Sigma$ is defined as the fourfold integration $\int d\Sigma = \int_{-\infty}^{+\infty} d\mathbf{v} \int_0^\infty dt_3 \int_0^\infty dt_2 \int_0^\infty dt_1$.

IV. THE PURELY HOMOGENEOUSLY BROADENED MEDIUM

A. $\tau > 0$

1. Nonlinear response at field level

In lifetime-broadened three-level atoms (Doppler-free approximation $\mathbf{k}_i \cdot \mathbf{v} \approx 0$ and $\mathbf{k}_i' \cdot \mathbf{v} \approx 0$) and $\tau > 0$, Eqs. (3)–(7) reduce to

$$P_1 = S_1(\mathbf{r})\exp[-i(\omega_3 t + \omega_1 \tau)]\frac{1}{\Gamma_{10} + i\Delta_3}\frac{1}{\Gamma_0}\left(\frac{e^{-\alpha_1 \tau}}{\Gamma_{10} - \alpha_1 + i\Delta_1} - \frac{2\alpha_1 e^{-(\Gamma_{10} + i\Delta_1)\tau}}{(\Gamma_{10} + i\Delta_1)^2 - \alpha_1^2}\right), \tag{8}$$

$$P_2 = S_1(\mathbf{r})\exp[-i(\omega_3 t + \omega_1 \tau)]\frac{1}{\Gamma_{10} + i\Delta_3}\frac{1}{\Gamma_0}\frac{e^{-\alpha_1 \tau}}{\Gamma_{10} + \alpha_1 - i\Delta_1}, \tag{9}$$

$$P_3 = S_1(\mathbf{r})\exp[-i(\omega_3 t + \omega_1 \tau)]\frac{1}{\Gamma_{10} + i\Delta_3}\frac{1}{\Gamma_1}\left(\frac{e^{-\alpha_1 \tau}}{\Gamma_{10} - \alpha_1 + i\Delta_1} - \frac{2\alpha_1 e^{-(\Gamma_{10}+i\Delta_1)\tau}}{(\Gamma_{10} + i\Delta_1)^2 - \alpha_1^2}\right), \tag{10}$$

$$P_4 = S_1(\mathbf{r})\exp[-i(\omega_3 t + \omega_1 \tau)]\frac{1}{\Gamma_{10} + i\Delta_3}\frac{1}{\Gamma_1}\frac{e^{-\alpha_1 \tau}}{\Gamma_{10} + \alpha_1 - i\Delta_1}, \tag{11}$$

$$P_5 = S_2(\mathbf{r})\exp[-i(\omega_3 t - \omega_2 \tau)]\frac{1}{\Gamma_{10} + i\Delta_3}\frac{1}{\Gamma_{10} + \alpha_2 + i\Delta_3} \times \frac{e^{-\alpha_2 \tau}}{\Gamma_{20} + i(\Delta_3 + \Delta_2)}. \tag{12}$$

Thus P_1 and P_3 with radiation-matter detuning oscillation (RDO) show both atom and light responses together, but P_2, P_4, and P_5 without RDO show light response alone (without $e^{-(\Gamma_{10}+i\Delta_1)\tau}$ or $e^{-(\Gamma_{20}+i\Delta_2+i\Delta_3)\tau}$ τ-dependent decay factors). In the limit of weak noisy fields and in the limit of zero correlation time of the noisy lights, the decay of the DFWM signal yields the dephasing time Γ_{10} of the atomic medium. The one-photon DFWM and two-photon NDFWM complex susceptibilities χ_A and χ_B at ω_3 ($\omega_3 \approx \Omega_1$) are obtained from the third-order polarizations P_A and P_B, respectively, as follows:

$$\chi_A(\tau, \Delta_i, \alpha_1) = \frac{P_A}{\varepsilon_0 \langle E_1 (E_1')^* \rangle E_3} = \frac{\psi_1(\Gamma_0 + \Gamma_1)}{(\Gamma_{10} + i\Delta_3)\Gamma_0\Gamma_1}\left(\frac{1}{\Gamma_{10} + \alpha_1 - i\Delta_1} + \frac{1}{\Gamma_{10} - \alpha_1 + i\Delta_1} - \frac{2\alpha_1 e^{-(\Gamma_{10}+i\Delta_1-\alpha_1)\tau}}{(\Gamma_{10} + i\Delta_1)^2 - \alpha_1^2}\right), \tag{13}$$

$$\chi_B(\Delta_i, \alpha_2) = \frac{P_B}{\varepsilon_0 \langle E_2^* E_2' \rangle E_3} = \frac{\psi_2}{\Gamma_{10} + i\Delta_3}\frac{1}{\Gamma_{10} + \alpha_2 + i\Delta_3}\frac{1}{\Gamma_{20} + i(\Delta_3 + \Delta_2)}, \tag{14}$$

where $\psi_1 = -iN\mu_1^4/\varepsilon_0\hbar^3$ and $\psi_2 = -iN\mu_1^2\mu_2^2/\varepsilon_0\hbar^3$.

The complex susceptibilities are greatly modified by the color-locked noisy fields. Specifically, χ_A and χ_B strongly depend on the linewidth α_i and time delay τ in broadband, while they become independent of α_i and τ in narrowband. In the cw limit ($\alpha_i = 0$), the imaginary part and real part of χ_A or χ_B can correspond to nonmodified nonlinear absorption and dispersion. For the absorption curves, positive (negative) values indicate gain (absorption). The signal response of FWM has also been calculated previously in four-level double-Λ cold atoms [3]. The anomalous dispersion generally corresponds to strong absorption of the medium. Close inspection of Eq. (14) shows that when α_2/Γ_{10}^a controllably decreases to the cw case ($\alpha_2/\Gamma_{10}^a = 0$), the absorption will increase, and the slope of the normal dispersion curve will dramatically increase at near resonance $\Delta_2/\Gamma_{10} = 0$ too (Fig. 3). Moreover, near the two-photon transition, there is large induced nonlinear amplification (Im χ_B negative) and Re χ_B is large and can have either sign.

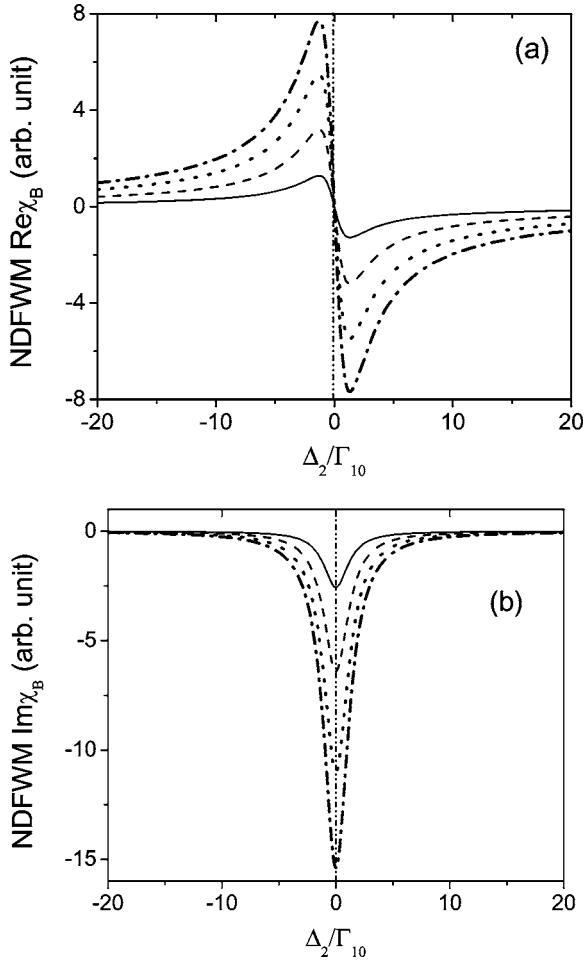

FIG. 3. Nonlinear dispersion (a) and absorption (b) versus Δ_2/Γ_{10} for Eq. (14). $\Gamma_{20}/\Gamma_{10} = 1.3$, $\Delta_3/\Gamma_{10} = -0.001$, and $\alpha_2/\Gamma_{10} = 0$ (cw case) (dash-dotted curve), 700 (dotted curve), 1200 (dashed curve), and 2000 (solid curve).

The expression for χ_B, which is responsible for the modification of the nonmodified nonlinear absorption-dispersion profile, arises in the bare-state formalism from a two-photon-induced coherence between levels $|0\rangle$ and $|2\rangle$, i.e., a nonzero matrix element $\rho_{20}^{(2)}$. Clearly, even for an atom at rest ($v = 0$), the color-locking characteristic of the noisy light modifies the normal susceptibility in a nontrivial way, which cannot be simply characterized as either a mere level shift or a broadening of the resonances. The phase dispersion

$$\theta_B(\Delta_2, \Delta_3, \alpha_2) = \tan^{-1}\left(\frac{(\Gamma_{10}^2 - \Delta_3^2)(\alpha_2 + \Gamma_{20}) - 2\Gamma_{10}\Delta_3(\Delta_2 + \Delta_3)}{2\Gamma_{10}\Delta_3(\alpha_2 + \Gamma_{20}) + (\Gamma_{10}^2 - \Delta_3^2)(\Delta_2 + \Delta_3)}\right)$$

of $\chi_B = |\chi_B| e^{i\theta_B}$ can be obtained simply from Eq. (14).

2. Nonlinear response at intensity level

The phase-sensitive detection of two-photon NDFWM is based on the polarization interference between two FWM processes. Since optical fields oscillate too quickly for direct detection, they must be measured by beating with another field with similar frequency. There are two ways to measure the nonlinear susceptibility of NDFWM experimentally. One is the conventional detection in which the NDFWM polarization P_B is measured at its own absolute square, $P_B(P_B)^*$. The two-photon NDFWM signal intensity is proportional to $|\chi_B|^2$ and all phase information of χ_B has been lost. The second way to measure χ_B is to introduce another polarization P_A (called a reference signal or local oscillator) designed in frequency and wave vector to conjugate in its complex representation with the P_B polarization of interest. Thus, in this heterodyne case, the signal photons are derived from $(P_A+P_B)[(P_A)^*+(P_B)^*]$ or $I_{heterodyne}\propto\chi_B$ (the signal is linear rather than quadratic). In heterodyne-detected FWM, phase information is retained and one can take a full measure of the complex susceptibility, including its phase. The phase of the induced complex polarization $P^{(3)}=P_A+P_B$ determines how its energy will partition between the absorbed or emitted active spectroscopy and the passive spectroscopy with a new launched field spectrum [11]. The ASPB intensity can be obtained as follows:

$$\begin{aligned} I(\tau,\Delta_i,\alpha_i) &\propto P_AP_A^*+P_BP_B^*+P_AP_B^*+P_A^*P_B \\ &= \eta_1|\chi_A|^2e^{-2\alpha_1\tau}+\eta_2|\chi_B|^2e^{-2\alpha_2\tau} \\ &\quad +2\eta_{12}|\chi_A||\chi_B|e^{-(\alpha_1+\alpha_2)\tau}\cos(\theta_A-\theta_B+\theta_R). \end{aligned} \tag{15}$$

Here $\chi_A=|\chi_A|e^{i\theta_A}=|\chi_A|\cos\theta_A+i|\chi_A|\sin\theta_A$, $\chi_B=|\chi_B|e^{i\theta_B}=|\chi_B|\cos\theta_B+i|\chi_B|\sin\theta_B$, $\theta_R=\Delta\mathbf{k}\cdot\mathbf{r}-(\omega_1+\omega_2)\tau$, $\Delta\mathbf{k}=(\mathbf{k}_1-\mathbf{k}_1')-(\mathbf{k}_2'-\mathbf{k}_2)$, $\eta_1=\varepsilon_0^2\varepsilon_1^2(\varepsilon'_1)^2\varepsilon_3^2$, $\eta_2=\varepsilon_0^2\varepsilon_2^2(\varepsilon'_2)^2\varepsilon_3^2$, and $\eta_{12}=\varepsilon_0^2\varepsilon_1(\varepsilon'_1)^*\varepsilon'_2\varepsilon_2^*\varepsilon_3^2$.

Although the complex susceptibilities (nonlinear responses) are greatly modified by the color-locked noisy fields, they can still be obtained effectively in the ideal limit. In the heterodyne detection, we assume that $|P_A|^2\gg|P_B|^2$ at the intensity level ($|\chi_A|\gg|\chi_B|$ at the field level), so the reference signal (DFWM) originated from the ω_1 frequency components of the twin beams 1 and 2 is much larger than the NDFWM signal originated from the ω_2 frequency components of the twin beams 1 and 2:

$$\begin{aligned} I(\tau,\Delta_i,\alpha_i) &\propto \eta_1|\chi_A|^2e^{-2\alpha_1\tau}+2\eta_{12}|\chi_B||\chi_A|e^{-(\alpha_1+\alpha_2)\tau} \\ &\quad\times\cos(\theta_A-\theta_B+\theta_R). \end{aligned} \tag{16}$$

Equation (16) indicates that the sum-frequency ASPB signal of heterodyne detection is modulated with a frequency $\omega_1+\omega_2$ as τ is varied. The phase-coherent control of the light beams in ASPB is subtle. The phase of the ASPB signal strongly depends on the phase angle θ_B of χ_B. Such an ASPB can effectively be employed via optical heterodyne detection to yield the real and imaginary parts of χ_B. If we adjust the time delay τ and $\mathbf{r}$ such that $\theta_A+\theta_R=2n\pi$ {i.e., $\tau=[\theta_A(\tau)+\Delta\mathbf{k}\cdot\mathbf{r}-2n\pi]/(\omega_1+\omega_2)$, $\Delta\mathbf{k}\cdot r=0$, and the value of integer n depends on the sign of τ sensitively}, then

$$I(\Delta_2)\propto\eta_1|\chi_A|e^{-2\alpha_1\tau}+2\eta_{12}e^{-(\alpha_1+\alpha_2)\tau}\mathrm{Re}[\chi_B(\Delta_2)]. \tag{17}$$

However, if $\theta_A+\theta_R=(2n+1/2)\pi$ {i.e., $\tau=[\theta_A(\tau)+\Delta\mathbf{k}\cdot\mathbf{r}-2n\pi-\pi/2]/(\omega_1+\omega_2)$, $\Delta\mathbf{k}\cdot\mathbf{r}=0$}, we have

$$I(\Delta_2)\propto\eta_1|\chi_A|e^{-2\alpha_1\tau}+2\eta_{12}e^{-(\alpha_1+\alpha_2)\tau}\mathrm{Im}[\chi_B(\Delta_2)]. \tag{18}$$

In other words, by changing the time delay τ between different frequencies ω_1 and ω_2 we can obtain the real and the imaginary parts of $\chi_B(\Delta_2,\Delta_3)$. The subtle value of τ is generally determined by the gradual approach method from $\theta_A(\tau)+\theta_R(\tau)=2n\pi$ or $(2n+1/2)\pi$. Since $\Delta_1\approx\Delta_3$, this procedure is not good for determining $\chi_A(\Delta_1,\Delta_3)$, which is dramatically different with the polarization interference between two two-photon NDFWM processes [10].

B. $\tau<0$

In a homogeneously broadened three-level ladder-type system, when $\tau<0$, Eqs. (3)–(7) can be reduced to

$$P_1=S_1(\mathbf{r})\exp[-i(\omega_3t+\omega_1\tau)]\frac{1}{\Gamma_{10}+i\Delta_3}\frac{1}{\Gamma_0}\frac{e^{\alpha_1\tau}}{\Gamma_{10}+\alpha_1+i\Delta_1}, \tag{19}$$

$$P_2=S_1(\mathbf{r})\exp[-i(\omega_3t+\omega_1\tau)]\frac{1}{\Gamma_{10}+i\Delta_3}\frac{1}{\Gamma_0}\left(\frac{e^{\alpha_1\tau}}{\Gamma_{10}-\alpha_1-i\Delta_1}-\frac{2\alpha_1e^{(\Gamma_{10}-i\Delta_1)\tau}}{(\Gamma_{10}-i\Delta_1)^2-\alpha_1^2}\right), \tag{20}$$

$$P_3=S_1(\mathbf{r})\exp[-i(\omega_3t+\omega_1\tau)]\frac{1}{\Gamma_{10}+i\Delta_3}\frac{1}{\Gamma_1}\frac{e^{\alpha_1\tau}}{\Gamma_{10}+\alpha_1+i\Delta_1}, \tag{21}$$

$$P_4=S_1(\mathbf{r})\exp[-i(\omega_3t+\omega_1\tau)]\frac{1}{\Gamma_{10}+i\Delta_3}\frac{1}{\Gamma_1}\left(\frac{e^{\alpha_1\tau}}{\Gamma_{10}-\alpha_1-i\Delta_1}-\frac{2\alpha_1e^{(\Gamma_{10}-i\Delta_1)\tau}}{(\Gamma_{10}-i\Delta_1)^2-\alpha_1^2}\right), \tag{22}$$

$$P_5=S_2(\mathbf{r})\exp[-i(\omega_3t-\omega_2\tau)]\frac{1}{(\Gamma_{10}+i\Delta_3)^2}\times\left(\frac{2\alpha_2e^{\tau(\Gamma_{20}+i\Delta_2+i\Delta_3)}}{\alpha_2^2-(\Gamma_{20}+i\Delta_2+i\Delta_3)^2}-\frac{e^{\alpha_2\tau}}{-\Gamma_{20}+\alpha_2-i\Delta_2-i\Delta_3}\right). \tag{23}$$

Thus P_2, P_4, and P_5 can show atom and light responses together, but P_1 and P_3 show only the light response. It is then straightforward to obtain χ_A and χ_B, as follows:

$$\chi_A(\tau,\Delta_i,\alpha_1)=\frac{P_A}{\varepsilon_0\langle E_1(E_1')^*\rangle E_3}$$
$$=\frac{\psi_1(\Gamma_0+\Gamma_1)}{(\Gamma_{10}+i\Delta_3)\Gamma_0\Gamma_1}\left(\frac{1}{\Gamma_{10}+\alpha_1+i\Delta_1}+\frac{1}{\Gamma_{10}-\alpha_1-i\Delta_1}-\frac{2\alpha_1 e^{(\Gamma_{10}-i\Delta_1-\alpha_1)\tau}}{(\Gamma_{10}-i\Delta_1)^2-\alpha_1^2}\right), \quad (24)$$

$$\chi_B(\tau,\Delta_i,\alpha_2)=\frac{P_B}{\varepsilon_0\langle E_2^* E_2'\rangle E_3}$$
$$=\frac{\psi_2}{(\Gamma_{10}+i\Delta_3)^2}\left(\frac{2\alpha_2 e^{(\Gamma_{20}+i\Delta_2+i\Delta_3-\alpha_2)\tau}}{\alpha_2^2-(\Gamma_{20}+i\Delta_2+i\Delta_3)^2}-\frac{1}{-\Gamma_{20}+\alpha_2-i\Delta_2-i\Delta_3}\right). \quad (25)$$

The one-photon DFWM and two-photon NDFWM complex susceptibilities χ_A and χ_B show atom and light responses together. When α_2/Γ_{10}^a controllably decreases [12] in Eq. (25) for $\tau<0$, the slope of the NDFWM dispersion curve will increase at near resonance; this term {the controllable slope of normal dispersion $d[\mathrm{Re}\,\chi_B(\Delta_2)]/d\omega_2|_{\Delta_2=0}>0$} can lead to the slow propagation of the phase-matched coherent NDFWM field and therefore the longer interaction length makes NDFWM more efficient [Figs. 3(a) and 4(a)]. Moreover, the NDFWM absorption curve becomes deeper as α_2/Γ_{10}^a decreases [Figs. 3(b) and 4(b)]. On the other hand, the RDO contrast of the NDFWM dispersion curve dramatically improves with increasing α_2/Γ_{10}^a. The RDO periods in the NDFWM dispersion and absorption curves also increase with reduction of $\Gamma_{10}|\tau|$ [Fig. 4(c)].

Although the complex susceptibilities are greatly modified by the color-locked noisy fields, they can still be obtained effectively in the ideal limit by employing heterodyne detection as

$$I(\tau,\Delta_i,\alpha_i)\propto \eta_1|\chi_A|^2e^{2\alpha_1\tau}+\eta_2|\chi_B|^2e^{2\alpha_2\tau}+2\eta_{12}|\chi_A||\chi_B|e^{(\alpha_1+\alpha_2)\tau}\cos(\theta_A-\theta_B+\theta_R). \quad (26)$$

If $|\chi_A|\gg|\chi_B|$ at field level, we then obtain

$$I(\tau,\Delta_i,\alpha_i)\propto \eta_1|\chi_A|e^{2\alpha_1\tau}+2\eta_{12}|\chi_B|e^{(\alpha_1+\alpha_2)\tau}\cos(\theta_A-\theta_B+\theta_R). \quad (27)$$

If we adjust the time delay τ and $\mathbf{r}$ such that $\theta_A+\theta_R=2n\pi$ {i.e., $\tau=[\theta_A(\tau)+\Delta\mathbf{k}\cdot\mathbf{r}-2n\pi]/(\omega_1+\omega_2)$}, then

$$I(\Delta_2)\propto \eta_1|\chi_A|e^{2\alpha_1\tau}+2\eta_{12}e^{(\alpha_1+\alpha_2)\tau}\mathrm{Re}[\chi_B(\Delta_2)]. \quad (28)$$

However, if $\theta_A+\theta_R=(2n+1/2)\pi$ {i.e., $\tau=[\theta_A(\tau)+\Delta\mathbf{k}\cdot\mathbf{r}-2n\pi-\pi/2]/(\omega_1+\omega_2)$}, we have

$$I(\Delta_2)\propto \eta_1|\chi_A|e^{2\alpha_1\tau}+2\eta_{12}e^{(\alpha_1+\alpha_2)\tau}\mathrm{Im}[\chi_B(\Delta_2)]. \quad (29)$$

The one-photon DFWM $|P_A|^2$ exhibits hybrid radiation-matter terahertz detuning damping oscillations at $\tau>0$ and $\tau<0$, while two-photon NDFWM $|P_B|^2$ shows RDO at τ

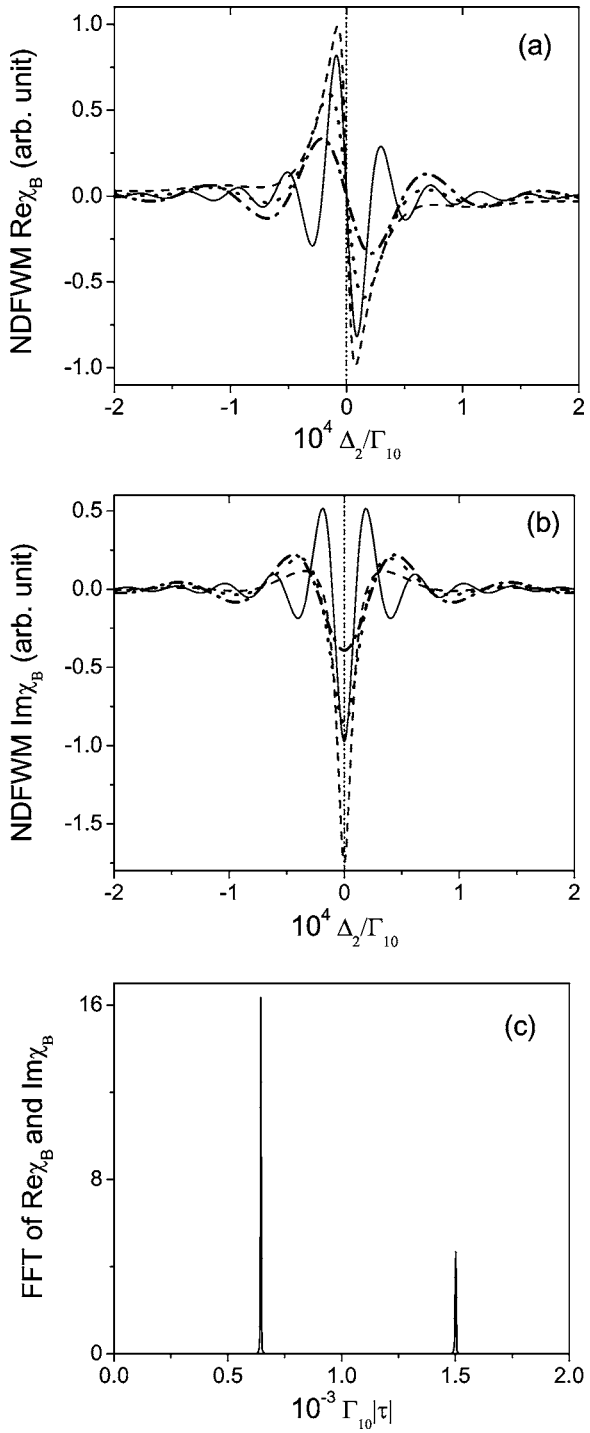

FIG. 4. NDFWM $\chi_B(\tau,\Delta_i,\alpha_2)$ response and its Fourier transform in a homogeneously broadened medium for $\tau<0$ processes. Nonlinear dispersion (a) and absorption (b) versus Δ_2/Γ_{10}. $\Gamma_{20}/\Gamma_{10}=1.3$, $\Delta_3/\Gamma_{10}=-0.001$. $\alpha_2/\Gamma_{10}=800$ and $\Gamma_{10}\tau=-0.000\,644\,2$ (dash-dotted curve), 2000 and $-0.000\,644\,2$ (dotted curve), 5000 and $-0.000\,644\,2$ (dashed curve), 2000 and -0.0015 (solid curve). (c) Fast Fourier transform (FFT) of dispersion and absorption curves; $\Gamma_{10}\tau=-0.000\,644\,2$ (high peak) and -0.0015 (low peak).

TABLE I. RDO frequencies on the terahertz scale of the self-coherence signal intensity of one-photon DFWM and two-photon NDFWM for three-state atoms in the lifetime-broadened and Doppler-broadened limits.

	DFWM		NDFWM	
Delay	$\tau>0$	$\tau<0$	$\tau>0$	$\tau<0$
Lifetime broadening	Δ_1	Δ_1	No	$\Delta_2+\Delta_3$
Large Doppler limit	Δ_1^a	No	No	Δ_2^a

<0 only (Table I). In the limit of the narrowband ($\alpha_1 \ll \Gamma_{10}$, $\alpha_2 \gg \Gamma_{20}$), and tail approximation ($\Gamma_{10}|\tau| \gg 1$), it is then straightforward to obtain

$$\chi_A = |\chi_A| e^{i\theta_A} = \psi_1 \frac{\Gamma_{10} + i\Delta_3}{\Gamma_{10}^2 + \Delta_3^2} \frac{\Gamma_0 + \Gamma_1}{\Gamma_0 \Gamma_1} \frac{2\Gamma_{10}}{\Gamma_{10}^2 + \Delta_1^2}$$

from Eqs. (13) and (24),

$$\chi_B = |\chi_B| e^{i\theta_B} = \frac{\psi_2}{(\Gamma_{10} + i\Delta_3)^2} \frac{1}{\Gamma_{20} + i(\Delta_3 + \Delta_2)}$$

from Eqs. (14) and (25), where $\theta_A = \tan^{-1}(\Gamma_{10}/\Delta_3)$. The real and imaginary parts of $\chi_A(\Delta_1, \Delta_3)$ or $\chi_B(\Delta_2, \Delta_3)$ are completely independent of α_i of the color-locked noisy lights and time delay τ, and correspond to the nonmodified nonlinear dispersion-absorption expressions. If $n=0$, we can obtain $\tau = \tan^{-1}(\Gamma_{10}/\Delta_3)/(\omega_1+\omega_2)$ for $\mathrm{Re}\,\chi_B(\Delta_2)$ in Eqs. (17) and (28), and $\tau = \tan^{-1}[(\Gamma_{10}/\Delta_3) - \pi/2]/(\omega_1+\omega_2)$ for $\mathrm{Im}\,\chi_B(\Delta_2)$ in Eqs. (18) and (29) (Figs. 3 and 4).

Since the phase-matched coherent NDFWM signal intensity $I_B \propto |E_B|^2 \approx |i\chi_B|^2 = (\mathrm{Re}\,\chi_B)^2 + (\mathrm{Im}\,\chi_B)^2$ [2], it makes the propagation characteristics of two-photon NDFWM pulse more complicated. Three key contributions are involved in the propagation characteristics of the NDFWM pulse [13]: a linear response term, a cross-Kerr (or self-Kerr) nonlinear term, and a phase-matched coherent NDFWM term (the dominant term). That is to say that the propagation characteristics of the NDFWM pulse are determined by all three of these contributions together. $\mathrm{Re}\chi_B$ and $\mathrm{Im}\,\chi_B$ may correspond to the phase-matched quasi cross-Kerr nonlinear index and the quasi two-photon absorption coefficient, respectively.

V. THE EXTREMELY DOPPLER-BROADENED LIMIT

When the atomic velocity distribution cannot be neglected, a straightforward semiclassical analysis shows that the contribution of the atoms with velocity v to the complex susceptibility of NDFWM is given by the heterodyne-detected ASPB. Under the extremely Doppler-broadened limit (i.e., $k_3 u \to \infty$, in the limit of pure inhomogeneous broadening), we have

$$\int_{-\infty}^{+\infty} d\mathbf{v}\, w(\mathbf{v}) \exp[-i\theta_I(\mathbf{v})] \approx 2\sqrt{\pi}\delta(t_3 - \xi_1 t_1)/k_3 u,$$

$$\int_{-\infty}^{+\infty} d\mathbf{v}\, w(\mathbf{v}) \exp[-i\theta_{II}(\mathbf{v})] \approx 2\sqrt{\pi}\delta(t_3 + \xi_1 t_1)/k_3 u,$$

$$\int_{-\infty}^{+\infty} d\mathbf{v}\, w(\mathbf{v}) \exp[-i\theta_{III}(\mathbf{v})] \approx 2\sqrt{\pi}\delta[t_3 + t_1 - (\xi_2 - 1)t_2]/k_3 u,$$

where $\xi_1 = k_1/k_3$, $\xi_2 = k_2/k_3 > 1$ for the two-photon coherence effect.

A. $\tau > 0$

1. Nonlinear response at field level

It is then straightforward to obtain the third-order polarizations of DFWM and NDFWM as follows:

$$P_1 = \frac{2\sqrt{\pi}}{k_3 u} S_1(\mathbf{r}) \exp[-i(\omega_3 t + \omega_1 \tau)] \frac{1}{\Gamma_0} \left(\frac{e^{-\alpha_1 \tau}}{\Gamma_{10}^a - \alpha_1 + i\Delta_1^a} + \frac{2\alpha_1 e^{-(\Gamma_{10}^a + i\Delta_1^a)\tau}}{\alpha_1^2 - (\Gamma_{10}^a + i\Delta_1^a)^2} \right), \tag{30}$$

$$P_3 = \frac{2\sqrt{\pi}}{k_3 u} S_1(\mathbf{r}) \exp[-i(\omega_3 t + \omega_1 \tau)] \frac{1}{\Gamma_1} \left(\frac{e^{-\alpha_1 \tau}}{\Gamma_{10}^a - \alpha_1 + i\Delta_1^a} + \frac{2\alpha_1 e^{-(\Gamma_{10}^a + i\Delta_1^a)\tau}}{\alpha_1^2 - (\Gamma_{10}^a + i\Delta_1^a)^2} \right), \tag{31}$$

$$P_5 = \frac{2\sqrt{\pi}}{k_3 u} S_2(\mathbf{r}) \exp[-i(\omega_3 t - \omega_2 \tau)] \frac{(\xi_2 - 1) e^{-\alpha_2 \tau}}{(\Gamma_{20}^a + \alpha_2 + i\Delta_2^a)^2},$$

$$P_2 = P_4 = 0. \tag{32}$$

Here, $\Gamma_{10}^a = \Gamma_{10} + \xi_1 \Gamma_{10}$, $\Delta_1^a = \Delta_1 + \xi_1 \Delta_3$; $\Gamma_{20}^a = \Gamma_{20} + (\xi_2 - 1)\Gamma_{10}$, and $\Delta_2^a = \Delta_2 + \xi_2 \Delta_3$.

Thus P_1 and P_3 with both atom and light responses lead to the one-photon DFWM $|P_1 + P_3|^2$ exhibiting hybrid radiation-matter terahertz detuning damping oscillations (Fig. 5), while P_5 with light response alone cannot cause RDO in the two-photon NDFWM $|P_5|^2$. The corresponding complex susceptibilities χ_A and χ_B are obtained from the third-order polarizations $P_A = P_1 + P_3$ and $P_B = P_5$, respectively, as follows:

$$\chi_A(\tau, \Delta_1^a, \alpha_1) = \frac{P_A}{\varepsilon_0 \langle E_1 (E_1')^* \rangle E_3} = \frac{2\sqrt{\pi}\psi_1}{k_3 u} \frac{\Gamma_0 + \Gamma_1}{\Gamma_0 \Gamma_1} \left(\frac{1}{\Gamma_{10}^a - \alpha_1 + i\Delta_1^a} + \frac{2\alpha_1 e^{-(\Gamma_{10}^a + i\Delta_1^a - \alpha_1)\tau}}{\alpha_1^2 - (\Gamma_{10}^a + i\Delta_1^a)^2} \right), \tag{33}$$

$$\chi_B(\Delta_2^a, \alpha_2) = \frac{P_B}{\varepsilon_0 \langle E_2^* E_2' \rangle E_3} = \frac{2\sqrt{\pi}\psi_2}{k_3 u} \frac{\xi_2 - 1}{(\Gamma_{20}^a + \alpha_2 + i\Delta_2^a)^2}. \tag{34}$$

$\chi_B(\Delta_2^a, \alpha_2) = |\chi_B| e^{i\theta_B}$ is completely independent of τ, and close to the nonmodified nonlinear dispersion-absorption ex-

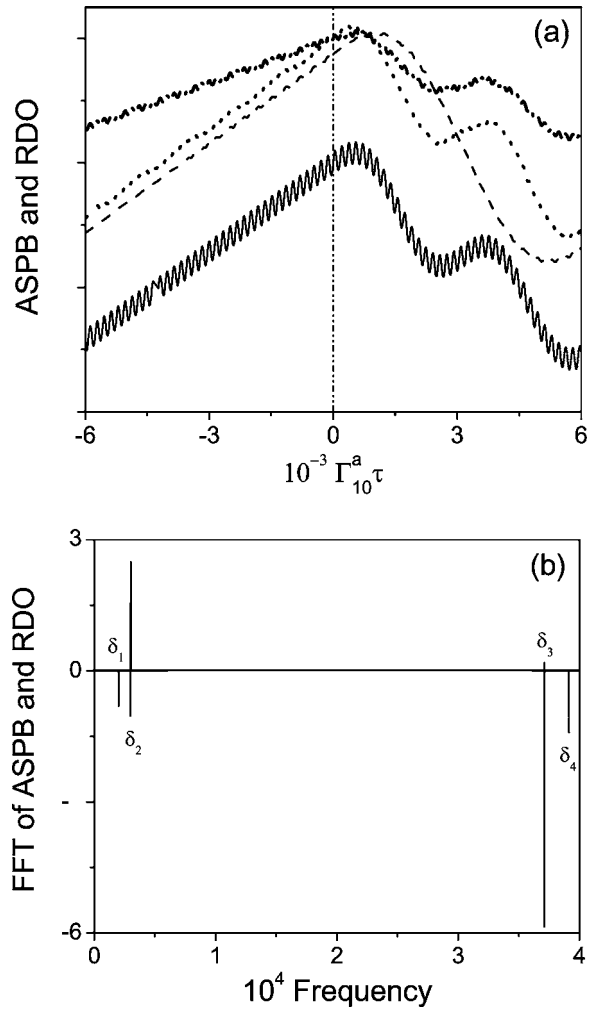

FIG. 5. Attosecond polarization beat, RDO, and their Fourier transforms in the extremely Doppler-broadened medium. (a) ASPB and RDO versus $\Gamma^a_{10}\tau$. $\alpha_2/\Gamma^a_{10}=0.6$, $\xi_2=2$, $\Gamma_0/\Gamma^a_{10}=\Gamma_1/\Gamma^a_{10}=0.5$, $\Gamma^a_{20}/\Gamma^a_{10}=1$, $(\omega_2+\omega_1)/\Gamma^a_{10}=37\,104.535$. $\alpha_1/\Gamma^a_{10}=0.3$, $\Delta^a_1/\Gamma^a_{10}=2000$, and $\Delta^a_2/\Gamma^a_{10}=3000$ (dash-dotted curve), 0.6, 2000, and 3000 (dotted curve), 0.6, 1000, and 3000 (dashed curve) and 0.6, 2000, and 1500 (solid curve). (b) FFT of ASPB and RDO for dash-dotted and dotted curves. The line positions δ_i $(i=1,2,3,4)$ correspond to Δ^a_1/Γ^a_{10}, Δ^a_2/Γ^a_{10}, $(\omega_2+\omega_1)/\Gamma^a_{10}$, $(\omega_2+\omega_1+\Delta^a_1)/\Gamma^a_{10}$, and $(\omega_2+\omega_1+\Delta^a_2)/\Gamma^a_{10}$ values, respectively.

pression, where the phase dispersion $\theta_B(\Delta^a_2,\alpha_2)=\tan^{-1}[(\Gamma^a_{20}+\alpha_2)/\Delta^a_2]$ and modulus $|\chi_B|=i\psi_2(\xi_2-1)/[(\Gamma^a_{20}+\alpha_2)^2+(\Delta^a_2)^2]$. The real and imaginary parts of $\chi_B(\Delta^a_2,\alpha_2)$ are given by the odd function (on Δ^a_2)

$$\mathrm{Re}\ \chi_B=\frac{2\sqrt{\pi}\psi_2}{ik_3u}\frac{(\xi_2-1)\Delta^a_2}{(\Gamma^a_{20}+\alpha_2)^2+(\Delta^a_2)^2}$$

and the even function (on Δ^a_2)

$$\mathrm{Im}\ \chi_B=\frac{2\sqrt{\pi}\psi_2}{ik_3u}\frac{(\xi_2-1)(\Gamma^a_{20}+\alpha_2)}{(\Gamma^a_{20}+\alpha_2)^2+(\Delta^a_2)^2},$$

respectively.

However, in the general case, χ_A and χ_B will strongly depend on the linewidth α_i and time delay τ in broadband (that is to say that the complex susceptibilities are greatly modified by the color-locked noisy fields), while they become independent of α_i and time delay τ in narrowband. In the cw limit $(\alpha_i=0)$, the real part and imaginary parts of χ_A or χ_B can correspond to the nonmodified nonlinear dispersion and absorption, respectively.

2. Nonlinear response at intensity level

In the extreme Doppler-broadened ASPB, using Eqs. (30)–(34) we obtain

$$I(\tau,\Delta^a_i,\alpha_i)\propto|P_A+P_B|^2=|P_A|^2+|P_B|^2+P_AP_B^*+P_A^*P_B, \tag{35}$$

where

$$P_A=\frac{2\sqrt{\pi}}{k_3u}S_1(r)\exp[-i(\omega_3t+\omega_1\tau)]\frac{\Gamma_0+\Gamma_1}{\Gamma_0\Gamma_1}\left(\frac{e^{-\alpha_1\tau}}{\Gamma^a_{10}-\alpha_1+i\Delta^a_1}+\frac{2\alpha_1e^{-(\Gamma^a_{10}+i\Delta^a_1)\tau}}{\alpha_1^2-(\Gamma^a_{10}+i\Delta^a_1)^2}\right)$$

(DFWM at field level) and

$$P_B=\frac{2\sqrt{\pi}}{k_3u}S_2(r)\exp[-i(\omega_3t-\omega_2\tau)]\frac{(\xi_2-1)^2e^{-\alpha_2\tau}}{(\Gamma^a_{20}+\alpha_2+i\Delta^a_2)^2}$$

(NDFWM at field level). Generally, the ASPB can be viewed as the sum of three contributions: $|P_A|^2=\eta_1|\chi_A|^2e^{-2\alpha_1\tau}$ (one-photon DFWM signal at intensity level), $|P_B|^2=\eta_2|\chi_B|^2e^{-2\alpha_2\tau}$ (two-photon NDFWM signal at intensity level), and $P_AP_B^*+P_A^*P_B=2\eta_{12}|\chi_A||\chi_B|e^{-(\alpha_1+\alpha_2)\tau}\cos(\theta_A-\theta_B+\theta_R)$ (cross term between DFWM and NDFWM at intensity level).

Similar to the previous discussions in Eqs. (15)–(18), we can write

$$I(\tau,\Delta^a_i,\alpha_i)\propto|P_A|^2+P_AP_B^*+P_A^*P_B=\eta_1|\chi_A|^2e^{-2\alpha_1\tau}+2\eta_{12}|\chi_A|\times|\chi_B|e^{-(\alpha_1+\alpha_2)\tau}\cos(\theta_A-\theta_B+\theta_R), \tag{36}$$

$$I(\Delta^a_2)\propto\eta_1|\chi_A|^2e^{-2\alpha_1\tau}+2\eta_{12}|\chi_A|e^{-(\alpha_1+\alpha_2)\tau}|\chi_B(\Delta^a_2)|\cos[\theta_B(\Delta^a_2)], \tag{37}$$

$$I(\Delta^a_2)\propto\eta_1|\chi_A|^2e^{-2\alpha_1\tau}+2\eta_{12}|\chi_A|e^{-(\alpha_1+\alpha_2)\tau}|\chi_B(\Delta^a_2)|\sin[\theta_B(\Delta^a_2)]. \tag{38}$$

Due to adding the local oscillator intensity in Eqs. (37) and (38), the dispersion and absorption profiles (Fig. 6) only show positive values compared with Fig. 3. After one subtracts the local oscillator background $|P_A|^2$ from them, they then become in good agreement with Fig. 3. In other words, by changing the time delay τ of the heterodyne-detected ASPB signal we can obtain the real and imaginary parts of $\chi_B(\Delta^a_2)$.

The broadband limit (noisy-field coherence time $\tau_c\approx0$, or $\alpha_i\to\infty$) corresponds to "white" noise, characterized by a

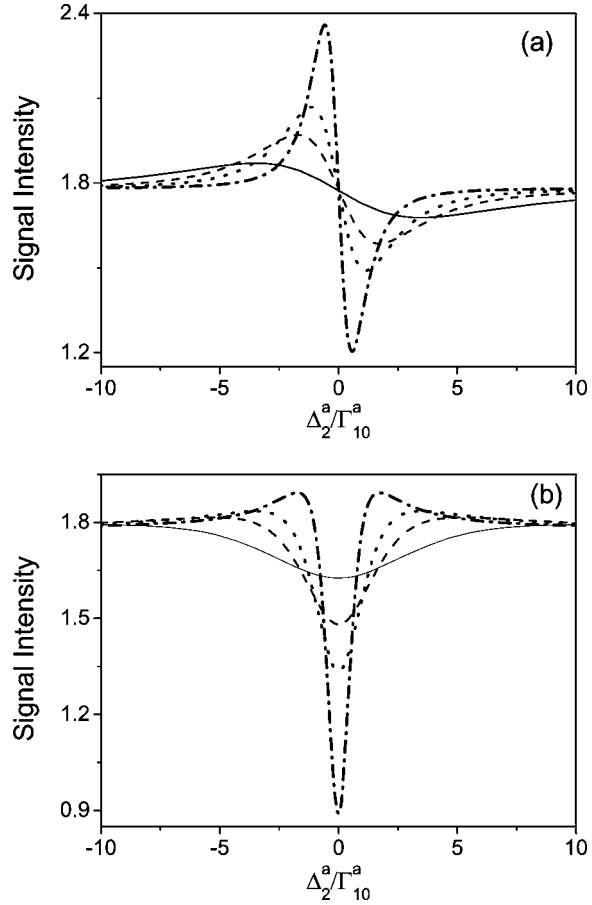

FIG. 6. The heterodyne detection spectra versus Δ_2^a/Γ_{10}^a of the ASPB (for the extremely-Doppler broadened three-state atoms $\tau>0$) with (a) $\tau=[\theta_A(\tau)+\Delta\mathbf{k}\cdot\mathbf{r}-2n\pi]/(\omega_1+\omega_2)$, $\Gamma_{10}^a\tau=0.000\,058\,9$ for the real part and (b) $\tau=[\theta_A(\tau)+\Delta\mathbf{k}\cdot\mathbf{r}-2n\pi-\pi/2]/(\omega_1+\omega_2)$, $\Gamma_{10}^a\tau=0.000\,039\,3$ for the imaginary part. The parameters are $\Gamma_0/\Gamma_{10}^a=\Gamma_1/\Gamma_{10}^a=0.5$, $\Gamma_{20}^a/\Gamma_{10}^a=1$, $(\omega_2+\omega_1)/\Gamma_{10}^a=37\,104.535$, $\xi_2=2$, $\Delta_1^a/\Gamma_{10}^a=-0.001$. $\alpha_1/\Gamma_{10}^a=\alpha_2/\Gamma_{20}^a=0$ (cw case) (dash-dotted curve), 1 (dotted curve), 2 (dashed curve), and 5 (solid curve).

δ-function time correlation or, alternatively, it possesses a constant spectral density. Under the large Doppler-broadening limit (i.e., $k_3u\to\infty$, inhomogeneous broadening limit) and broadband ($\alpha_1\gg\Gamma_{10}^a$ and $\alpha_2\gg\Gamma_{20}^a$) approximation, we can obtain

$$\chi_A(\Delta_1^a,\alpha_1,\tau)=\frac{2\sqrt{\pi}\psi_1}{k_3u}\frac{\Gamma_0+\Gamma_1}{\Gamma_0\Gamma_1}\left(\frac{1}{i\Delta_1^a-\alpha_1}+\frac{2\alpha_1 e^{-(\Gamma_{10}^a-\alpha_1+i\Delta_1^a)\tau}}{\alpha_1^2-(\Gamma_{10}^a+i\Delta_1^a)^2}\right)$$

and

$$\chi_B(\Delta_2^a,\alpha_2,\tau)=\frac{2\sqrt{\pi}\psi_2}{k_3u}\frac{(\xi_2-1)^2}{(\alpha_2+i\Delta_2^a)^2}$$

from Eqs. (33) and (34). These complex susceptibilities are greatly modified by the color-locked noisy field. That is to say that χ_A and χ_B strongly depend on the noisy-field parameter α_i and time delay τ in broadband.

B. $\tau<0$

In an inhomogeneously broadened three-level ladder-type system, we can obtain

$$P_1=\frac{2\sqrt{\pi}}{k_3u}S_1(\mathbf{r})\exp[-i(\omega_3t+\omega_1\tau)]\frac{1}{\Gamma_0}\frac{e^{\alpha_1\tau}}{\Gamma_{10}^a+\alpha_1+i\Delta_1^a},\tag{39}$$

$$P_3=\frac{2\sqrt{\pi}}{k_3u}S_1(\mathbf{r})\exp[-i(\omega_3t+\omega_1\tau)]\frac{1}{\Gamma_1}\frac{e^{\alpha_1\tau}}{\Gamma_{10}^a+\alpha_1+i\Delta_1^a},\tag{40}$$

$$P_5=\frac{2\sqrt{\pi}}{k_3u}S_2(\mathbf{r})\exp[-i(\omega_3t-\omega_2\tau)]\left(\frac{(\xi_2-1)^2e^{\alpha_2\tau}}{[\alpha_2-(\Gamma_{20}^a+i\Delta_2^a)]^2}+\frac{\tau[(\Gamma_{20}^a+i\Delta_2^a)^2-\alpha_2{}^2]-2(\Gamma_{20}^a+i\Delta_2^a)}{[\alpha_2{}^2-(\Gamma_{20}^a+i\Delta_2^a)^2]^2}\times 2\alpha_2(\xi_2-1)^2e^{(\Gamma_{20}^a+i\Delta_2^a)\tau}\right),$$

$$P_2=P_4=0.\tag{41}$$

Thus P_1 and P_3 with light response alone cannot cause the RDO of the one-photon DFWM $|P_A|^2$, while P_5 with both atom and light responses leads to the two-photon NDFWM $|P_B|^2$ exhibiting hybrid radiation-matter terahertz detuning damping oscillations (Fig. 5). Due to the effects of noisy-field color locking, in the limit of zero correlation time of the noisy light, the decay of the NDFWM signal yields a dephasing time Γ_{20}^a of the atomic medium. The maximum of the Doppler-broadened NDFWM $|P_B|^2$ is shifted from zero time delay compared with the DFWM $|P_A|^2$. Close inspection of $|P_B|^2$ shows that the maximum of the NDFWM signal occurs at $\tau=1/\Gamma_{20}^a$. More specifically, the NDFWM profile becomes asymmetric due to the τ-dependent coefficient of the second term in Eq. (41) and the degree of asymmetry is determined by $(\Gamma_{20}^a)^{-1}$. It is then straightforward to obtain χ_A and χ_B as follows:

$$\chi_A(\Delta_1^a,\alpha_1)=\frac{P_A}{\varepsilon_0\langle E_1(E_1')^*\rangle E_3}=\frac{2\sqrt{\pi}\psi_1}{k_3u}\frac{\Gamma_0+\Gamma_1}{\Gamma_0\Gamma_1}\frac{1}{\Gamma_{10}^a+\alpha_1+i\Delta_1^a},\tag{42}$$

$$\chi_B(\tau,\Delta_2^a,\alpha_2)=\frac{P_B}{\varepsilon_0\langle E_2^*E_2'\rangle E_3}=\frac{2\sqrt{\pi}\psi_2}{k_3u}\left(\frac{(\xi_2-1)^2}{[\alpha_2-(\Gamma_{20}^a+i\Delta_2^a)]^2}+\frac{\tau[(\Gamma_{20}^a+i\Delta_2^a)^2-\alpha_2{}^2]-2(\Gamma_{20}^a+i\Delta_2^a)}{[\alpha_2{}^2-(\Gamma_{20}^a+i\Delta_2^a)^2]^2}\times 2\alpha_2(\xi_2-1)^2e^{(\Gamma_{20}^a-\alpha_2+i\Delta_2^a)\tau}\right).\tag{43}$$

One-photon DFWM $\chi_A(\Delta_1^a,\alpha_1)=|\chi_A|e^{i\theta_A}$ shows light response alone, while the two-photon NDFWM $\chi_B(\tau,\Delta_2^a,\alpha_2)$ shows atom and light responses together, where $|\chi_A|=2\sqrt{\pi}i\psi_1(\Gamma_0+\Gamma_1)/k_3u\Gamma_0\Gamma_1\sqrt{(\Gamma_{10}^a+\alpha_1)^2+(\Delta_1^a)^2}$ and θ_A

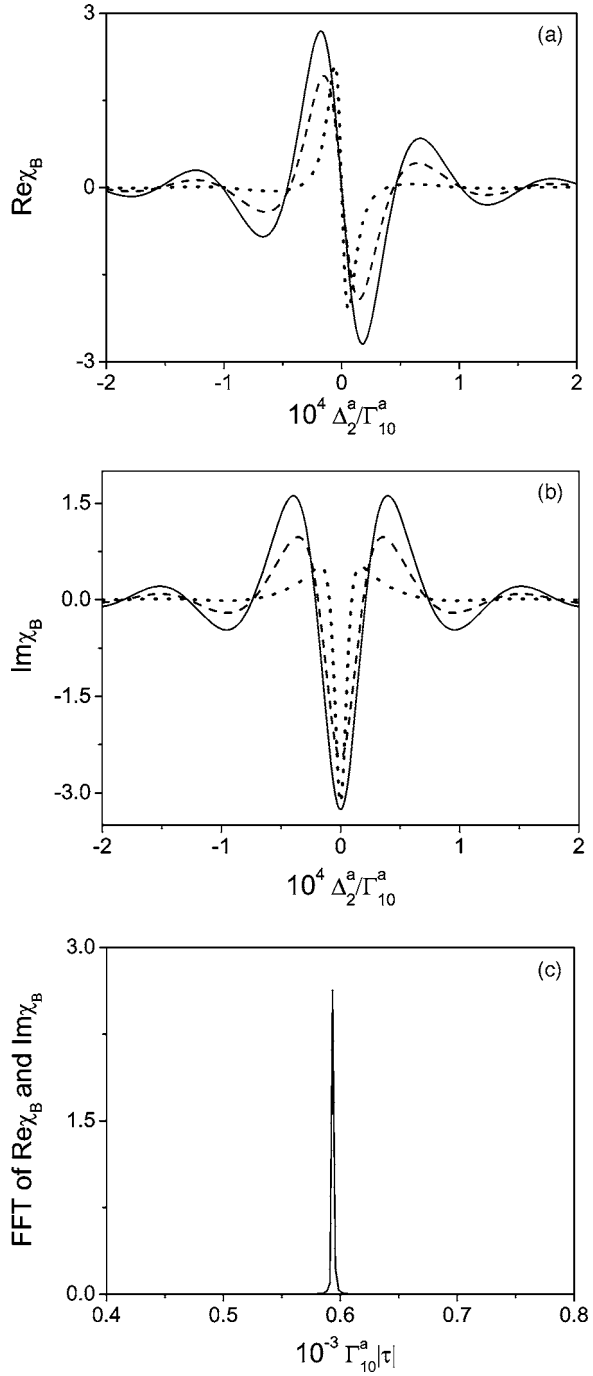

FIG. 7. NDFWM $\chi_B(\tau,\Delta_i^a,\alpha_2)$ response and its Fourier transform in the extremely Doppler-broadened three-state atoms for $\tau<0$. Nonlinear dispersion (a) and absorption (b) versus Δ_2^a/Γ_{10}^a. $\Gamma_{20}^a/\Gamma_{10}^a=1$, $\xi_2=2$, $\Gamma_{10}^a\tau=-0.000\,594$, $\alpha_2/\Gamma_{10}=1000$ (dotted curve), 3000 (dashed curve), and 4000 (solid curve). (c) FFT of dispersion and absorption curves, $\Gamma_{10}^a\tau=-0.000\,594$.

$=\tan^{-1}[(\Gamma_{10}^a+\alpha_1)/\Delta_1^a]$. The nonlinear dispersion slope decreases and absorption dip gets deeper, and their RDOs show strong competition versus the bandwidth increase of the color-locked noisy fields in Fig. 7. The strong RDO can wash out the slope reduction effect, or change its variation direction [Fig. 7(a)] and suppress the nonlinear absorption [Fig. 7(b)]. The color-locked noisy effects of incoherent fields can

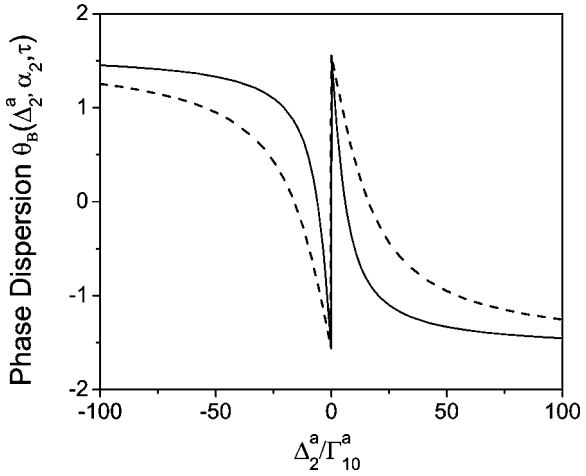

FIG. 8. Phase dispersion of two-photon NDFWM, $\theta_B(\Delta_2^a,\alpha_2,\tau)\sim\Delta_2^a$. The parameters are $\Gamma_{20}^a/\Gamma_{10}^a=1$, $\xi_2=2$, $\Gamma_{10}^a\tau=-0.000\,019\,6$. $\alpha_2/\Gamma_{10}^a=15$ (dashed curve) and 5 (solid curve).

lead to controllable change for third-order nonlinear response and obvious hybrid radiation-matter terahertz oscillation. Figure 8 shows the phase dispersion of the two-photon NDFWM including the influence of the color-locked noisy field.

Similar to Eqs. (26)–(29), we can obtain

$$I(\tau,\Delta_i^a,\alpha_i)\propto \eta_1|\chi_A|^2e^{2\alpha_1\tau}+\eta_2|\chi_B|^2e^{2\alpha_2\tau}+2\eta_{12}|\chi_A| \times|\chi_B|e^{(\alpha_1+\alpha_2)\tau}\cos(\theta_A-\theta_B+\theta_R), \tag{44}$$

$$I(\tau,\Delta_i^a,\alpha_i)\propto \eta_1|\chi_A|^2e^{2\alpha_1\tau}+2\eta_{12}|\chi_A||\chi_B|e^{(\alpha_1+\alpha_2)\tau} \times\cos(\theta_A-\theta_B+\theta_R), \tag{45}$$

$$I(\Delta_2^a)\propto \eta_1|\chi_A|^2e^{2\alpha_1\tau}+2\eta_{12}|\chi_A|e^{(\alpha_1+\alpha_2)\tau}|\chi_B(\Delta_2^a)|\cos[\theta_B(\Delta_2^a)], \tag{46}$$

$$I(\Delta_2^a)\propto \eta_1|\chi_A|^2e^{2\alpha_1\tau}+2\eta_{12}|\chi_A|e^{(\alpha_1+\alpha_2)\tau}|\chi_B(\Delta_2^a)|\sin[\theta_B(\Delta_2^a)]. \tag{47}$$

Because of the local oscillator intensity in Eqs. (46) and (47), the dispersion and absorption profiles (Fig. 9) have been upshifted by an amount $|P_A|^2$ compared with Fig. 7. After subtracting the local oscillator background from them, they become in good agreement with Fig. 7.

The one-photon DFWM $|P_1+P_3|^2$ exhibits hybrid radiation-matter terahertz detuning damping oscillations at $\tau>0$, while the two-photon NDFWM $|P_5|^2$ shows RDO at $\tau<0$ (Table I). The modified two-photon third-order absorption and dispersion can be controlled coherently by noisy-light color-locking bandwidth, frequency detuning, and time delay. In the narrowband and tail approximation ($\alpha_1\ll\Gamma_{10}^a$, $\alpha_2\ll\Gamma_{20}^a$, and $\Gamma_{10}^a|\tau|\gg1$), it is then straightforward to obtain

$$\chi_A(\Delta_1^a)=|\chi_A|e^{i\theta_A}=\frac{2\sqrt{\pi}\psi_1}{k_3u}\frac{\Gamma_0+\Gamma_1}{\Gamma_0\Gamma_1}\frac{1}{\Gamma_{10}^a+i\Delta_1^a}$$

from Eqs. (33) and (42),

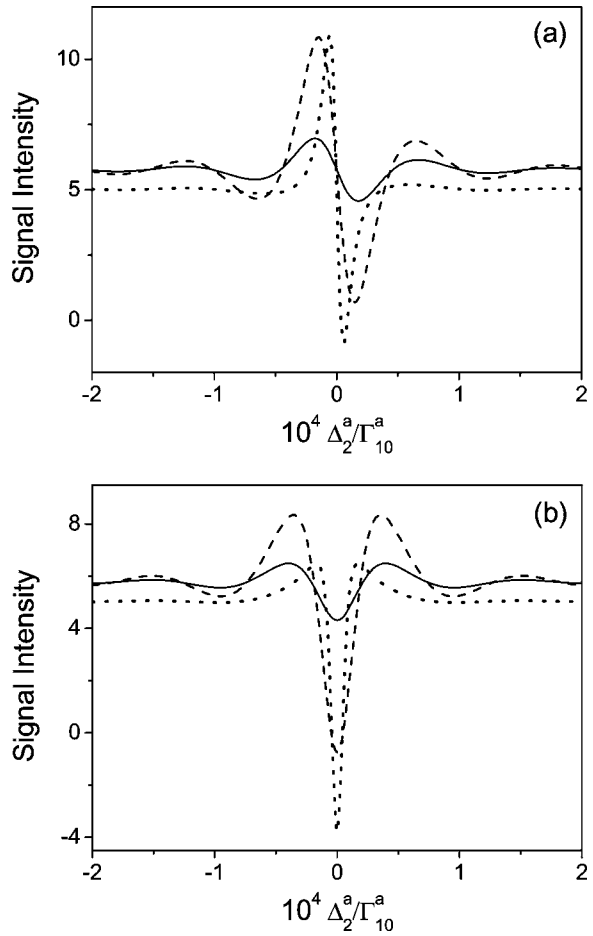

FIG. 9. The heterodyne detection spectra versus Δ_2^a/Γ_{10}^a of the ASPB (for the extremely-Doppler broadened three-state atom $\tau<0$) with (a) $\tau=[\theta_A(\tau)+\Delta\mathbf{k}\cdot\mathbf{r}-2n\pi]/(\omega_1+\omega_2)$, $\Gamma_{10}^a\tau=-0.000\,594$ for the real part and (b) $\tau=[\theta_A(\tau)+\Delta\mathbf{k}\cdot\mathbf{r}-2n\pi-\pi/2]/(\omega_1+\omega_2)$, $\Gamma_{10}^a\tau=-0.000\,039\,3$ for the imaginary part. The parameters are $\Gamma_0/\Gamma_{10}^a=\Gamma_1/\Gamma_{10}^a=0.5$, $\Gamma_{20}^a/\Gamma_{10}^a=1$, $(\omega_2+\omega_1)/\Gamma_{10}^a=37\,104.535$, $\xi_2=2$, $\Delta_1^a/\Gamma_{10}^a=-0.001$, $\alpha_1/\Gamma_{10}^a=1000$. $\alpha_2/\Gamma_{10}^a=1000$ (dotted curve), 3000 (dashed curve), and 4000 (solid curve). The dotted curve has been scaled by a factor 0.03.

$$\chi_B(\Delta_2^a)=|\chi_B|e^{i\theta_B}=\frac{2\sqrt{\pi}\psi_2}{k_3u}\frac{(\xi_2-1)^2}{(\Gamma_{20}^a+i\Delta_2^a)^2}$$

from Eqs. (34) and (43), where $\theta_A=\tan^{-1}(\Gamma_{10}^a/\Delta_1^a)$ and $\theta_B=\tan^{-1}\{[(\Gamma_{20}^a)^2+(\Delta_2^a)^2]/2\Gamma_{20}^a\Delta_2^a\}$. The real part and imaginary parts of $\chi_A(\Delta_1^a)$ or $\chi_B(\Delta_2^a)$ are independent of α_i and τ, and correspond to the nonmodified quasi cross-Kerr nonlinear index and two-photon absorption coefficient. Due to the transcendental functions, the precise value of τ is generally determined by the gradual approach method from $\theta_A(\tau)+\theta_R(\tau)=2n\pi$ or $(2n+1/2)\pi$. If $n=0$, we can readily obtain $\tau=\tan^{-1}[(\Gamma_{10}^a/\Delta_1^a)/(\omega_1+\omega_2)]$ for Re $\chi_B(\Delta_2^a)$ in Eqs. (37) and (46), $\tau=\tan^{-1}\{[(\Gamma_{10}^a/\Delta_1^a)-\pi/2]/(\omega_1+\omega_2)\}$ for Im $\chi_B(\Delta_2^a)$ in Eqs. (38) and (47).

Equations (35) and (44) contain rich dynamics of the color-locked noisy-field correlation effects [7,10,11], and the competition between attosecond ultrafast modulation and hybrid terahertz RDO. Close inspection of Eqs. (35) and (44) reveals four interesting observations (Fig. 5): (a) When α_1/Γ_{10}^a of the local oscillator and α_2/Γ_{10}^a of the two-photon NDFWM increase, the RDO contrast of DFWM and NDFWM will dramatically improve for $\Gamma_{10}^a\tau>0$ and $\Gamma_{10}^a\tau<0$, respectively; (b) if Δ_2^a/Γ_{10}^a increases, the attosecond beat modulation contrast will dramatically improve; (c) when Δ_1^a/Γ_{10}^a and Δ_2^a/Γ_{10}^a increase, the RDO oscillation periods of DFWM and NDFWM will decrease for $\Gamma_{10}^a\tau>0$ and $\Gamma_{10}^a\tau<0$, respectively; (d) the frequencies of RDO and ASPB can be read as [Fig. 5(c)] Δ_1^a/Γ_{10}^a, Δ_2^a/Γ_{10}^a, $(\omega_2+\omega_1)/\Gamma_{10}^a$, $(\omega_2+\omega_1+\Delta_1^a)/\Gamma_{10}^a$, and $(\omega_2+\omega_1+\Delta_2^a)/\Gamma_{10}^a$, which is the combination of $\Gamma_{10}^a\tau>0$ and $\Gamma_{10}^a\tau<0$ results (Table II). The detailed results of frequency analysis of RDO and ASPB are listed in Tables I and II.

VI. DISCUSSION AND CONCLUSION

As a time-domain technique, the main advantage of the ASPB technique over the conventional quantum beat technique is that the temporal resolution is not limited by the laser pulse width. With a laser pulse of nanosecond time scale duration, femto- or attosecond time scale modulations were observed [10]. We reported studies of attosecond polarization beats induced by the third-order susceptibility $\chi^{(3)}$. This effect was exploited to consider the phase of $\chi^{(3)}$ measurements in lifetime-broadened and extremely Doppler-broadened three-level atoms. The method presented here is simple to employ and can be applied to a large variety of materials in which backward FWM (phase conjugation) can be observed [9].

Specifically, let us consider the Na atom as a possible FWM system. We take, for instance, $|0\rangle=|3S_{1/2}\rangle$, $|1\rangle$

TABLE II. Ultrafast oscillation frequencies (period on the attosecond scale) and terahertz-scale RDO frequencies of the ASPB signal intensity for three-state atoms in the lifetime-broadened and Doppler broadened limits.

ASPB between DFWM and NDFWM			
Delay	$\tau>0$	$\tau<0$	Combination of $\tau>0$ and $\tau<0$
Lifetime broadening	Δ_1, $\omega_1+\omega_2$, $\Omega_1+\omega_2$	Δ_1, $\Delta_2+\Delta_3$, $\omega_1+\omega_2$, $\Omega_1+\omega_2$, $\omega_1+\Omega_2+\Delta_3$, $\Omega_1+\Omega_2+\Delta_3$	Δ_1, $\Delta_2+\Delta_3$, $\omega_1+\omega_2$, $\Omega_1+\omega_2$, $\omega_1+\Omega_2+\Delta_3$, $\Omega_1+\Omega_2+\Delta_3$
Large Doppler limit	Δ_1^a, $\omega_1+\omega_2$, $\Omega_1+\omega_2+\xi_1\Delta_3$	Δ_2^a, $\omega_1+\omega_2$, $\omega_1+\Omega_2+\xi_2\Delta_3$	Δ_1^a, Δ_2^a, $\omega_1+\omega_2$, $\Omega_1+\omega_2+\xi_1\Delta_3$, $\omega_1+\Omega_2+\xi_2\Delta_3$

$=|3P_{3/2}\rangle$, and $|2\rangle=|4D_{3/2,5/2}\rangle$. The respective transitions are $|0\rangle\rightarrow|1\rangle$ at 588.996 nm ($\Gamma_1^{-1}\approx 16.9$ ns, $\Gamma_{10}^{-1}\approx 5.7$ ps), and $|1\rangle\rightarrow|2\rangle$ at 568.822 nm, all accessible with non-transform-limited pulsed dye lasers operated in multiple longitudinal modes (typical color-locked chaotic fields). The ASPB signal in the present three-level atomic system not only exhibits 965 as ultrafast modulation [7,10,14], but also shows hybrid radiation-matter detuning damping oscillation at the terahertz scale (Tables I and II). The maximum of the two-photon NDFWM is shifted from zero time delay, and the signal also exhibits damping oscillations when the laser frequency is off resonant from the two-photon transition. This method can be useful for directly measuring $\chi^{(3)}$.

Two-color FWM of the attosecond polarization beat has been employed for studying the phase dispersion of $\chi^{(3)}$. This is a good way to measure the third-order susceptibility directly, especially its real and imaginary parts separately. Although our method is somewhat similar to the femtosecond polarization beats done in a solid by Ma *et al.* [6], we have shown that for two-photon resonance in a three-level atomic system one can obtain the phase dispersion of $\chi^{(3)}$ by simply measuring the phase change of the NDFWM signal modulation as the ω_2 detuning is varied. Moreover, the technique of using attosecond polarization beats to measure the third-order susceptibility has advantages over other (such as *Z*-scan) methods for atomic systems, because it can work with long atomic cells [2]. Generally speaking, our method can also be applied to study the phase dispersion of $\chi^{(3)}$ of the femtosecond polarization beats in gas-phase media.

In summary, we demonstrated a phase-sensitive technique to study the NDFWM in a three-level ladder-type atomic system. The reference signal is another DFWM signal, which propagates along the same optical path as the NDFWM signal. This point is very important since the reference signal always travels in basically the same direction, so it is much easier for mode matching and reducing the background (all other fields, linear processes, scattering, etc.). This method was used to investigate the phase dispersion of the third-order susceptibility and optical heterodyne detection of the two-photon NDFWM signal under various limits and conditions.

ACKNOWLEDGMENT

We acknowledge funding support from the National Science Foundation.

[1] M. Jain, H. Xia, G. Y. Yin, A. J. Merriam, and S. E. Harris, Phys. Rev. Lett. **77**, 4326 (1996); D. A. Braje, V. Balic, S. Goda, G. Y. Yin, and S. E. Harris, *ibid.* **93**, 183601 (2004).

[2] B. Lu, W. H. Burkett, and M. Xiao, Opt. Lett. **23**, 804 (1998); Y. Li and M. Xiao, *ibid.* **21**, 1064 (1996).

[3] H. Kang, G. Hernandez, and Y. F. Zhu, Phys. Rev. A **70**, 061804(R) (2004); **70**, 011801(R) (2004).

[4] H. Wang, D. Goorskey, and M. Xiao, Phys. Rev. Lett. **87**, 073601 (2001); H. Wang, D. J. Goorskey, and M. Xiao, Opt. Lett. **27**, 258 (2002).

[5] H. Kang and Y. F. Zhu, Phys. Rev. Lett. **91**, 093601 (2003).

[6] H. Ma, L. H. Acioli, A. S. L. Gomes, and C. B. de Araujo, Opt. Lett. **16**, 630 (1991); H. Ma, A. S. L. Gomes, and C. B. de Araujo, *ibid.* **17**, 1052 (1992); H. Ma and C. B. de Araujo, Phys. Rev. Lett. **71**, 3649 (1993).

[7] Y. P. Zhang, C. L. Gan, L. Li, R. Q. Ma, J. P. Song, T. Jiang, X. J. Yu, C. S. Li, H. Ge, and K. Q. Lu, Phys. Rev. A **72**, 013812 (2005); J. Opt. Soc. Am. B **22**, 694 (2005).

[8] D. DeBeer, E. Usadi, and S. R. Hartmann, Phys. Rev. Lett. **60**, 1262 (1988).

[9] P. M. Fu, X. Mi, Z. H. Yu, Q. Jiang, Y. P. Zhang, and X. F. Li, Phys. Rev. A **52**, 4867 (1995).

[10] Y. P. Zhang, C. B. de Araujo, and E. E. Eyler, Phys. Rev. A **63**, 043802 (2001); Y. P. Zhang, C. L. Gan, J. P. Song, X. J. Yu, R. Q. Ma, H. Ge, C. S. Li, and K. Q. Lu, *ibid.* **71**, 023802 (2005).

[11] N. Morita and T. Yajima, Phys. Rev. A **30**, 2525 (1984); D. J. Ulness, J. Phys. Chem. A **107**, 8111 (2003); T. F. Schulz, P. P. Aung, L. R. Weisel, K. M. Cosert, M. W. Gealy, and D. J. Ulness, J. Opt. Soc. Am. B **22**, 1052 (2005); J. C. Kirkwood, D. J. Ulness, and A. C. Albrecht, J. Phys. Chem. A **104**, 4167 (2000).

[12] W. H. Burkett, B. Lu, and M. Xiao, IEEE J. Quantum Electron. **33**, 2111 (1997).

[13] Y. P. Zhang, A. W. Brown, and M. Xiao (unpublished).

[14] M. Drescher, M. Hentschel, R. Kienberger, M. Uiberacker, V. Yakovlev, A. Scrinzi, Th. Westerwalbesloh, U. Kleineberg, U. Heinzmann, and F. Krausz, Nature (London) **419**, 803 (2002).